Memoirs of the Faculty of Engineering, Nagoya University
Vol. 33, No. 1 (1981)

ON THE PROCESS OF COMPONENTS-ROLLING

SHIGEAKI TSUTSUMI

Department of Mechanical Engineering

(Received May 30, 1981)

Abstract

This paper presents a comprehensive view of the components-rolling process attained by detailed observations.

In order to provide a fundamental approach to the rolling process of various rotational-type components, a series of experimental studies has been carried out. By means of experimental rolling of screw-like and gear-like components, features and shapes which blank cylinders come to develop in a process are observed in detail. In order to realize the characteristics of deformation, a method is taken in which experimental processes are examined comparatively by establishing a model process under some simple assumptions accepted as plausible. By this means, it becomes clear that a distortion observable in the cross sectional figure of a workpiece plays an important role in the rolling process.

For detecting the deformation of material during the process, the split plug buried in the workpiece is employed. By examining a distorted grid of the plug, a three dimensional pattern of the material flow has become clear for the first time. It has been proved that the central portion of the blank cylinders does deform so as to proceed the rolling action and this central deformation affects drastically the formation of functional features of the component. Efficacy of forming depends solely on the balance of these exo- and endo-deformations. On the basis of this deformation analysis, the mechanics of a rolling process is clarified and the fundamental controlling factors are pointed out.

CONTENTS

1. Introduction

The components-rolling is preferred by many factories as a method of producing various rotational-type components because of its high productivity and low noise. The rolling method can be adapted for various features such as screw threads, gears, splines, finned tubes, V-belt pulleys, balls, stepped shafts, thin tubes, twist drills, and so on, where the method can afford them many superior mechanical properties.

Although it is generally appreciated that components-rolling has proved economical on large-quantity production, similar savings and economics are often realized on small-lot production.

In the components-rolling, it is expected that the surface of the blank material is reformed exactly into an envelope of the die profiles, but an actual working condition is more complicated. Troubles in the components-rolling are brought about by somewhat particular inherency in the deformation which may be stated as follows.

(1) The freedom of disfiguration of a workpiece is fairly larger than that in the cutting process or other deformation processings such as sheet metal rolling, forging, extrusion, and so on. Accordingly, accuracy of the finished form of the components appears inherently difficult to control.

(2) During the process each die rotates relatively around an instantaneous center which moves on the surface of the work material, and the deformation work is caused by a couple of the tangential forces acting on the narrow contact zones. Therefore, it becomes important to characterize the deformation under such tools bearing in mind the rotative component of their movements so as to conform to the contact condition between tools and a work material.

(3) The whole work material or a part of it undergoes repeated plastic deformation which might be referred to as "plastic kneading". While the plastic kneading of a component can bring about a strengthening of the surface layer with the profit of diminution of surface roughness, the tool exercises plastic straining upon each element of the material causing it to pass through various phases of the stress field during each revolution and thus the material is strained cumulatively.

(4) Experience has shown that the rate of die penetration per bite affects considerably the behavior of material in respect to the formation of a feature. Any decisive datum, however, has not been drawn to date, and trial and error has been an inseparable part of the components-rolling.

Although many studies have been made on the rotary types of the forming process, an attempt has never been made in which various kinds of machine elements produced by rolling methods, such as thread screws, gears, and splines, could be taken up in a single research comprehensively. In the thread rolling, for example, optimum blank diameters[1] and rolling forces[2] were examined, and it was pointed out that an excessive amount of rolling decreased the fatigue strength[3]. In the gear rolling, investigators aimed at the accuracy of the tooth profile generated in various conditions[4]. In the cases of the cross rolling of a stepped shaft, rolling force was analyzed[5] and a crack which was initiated in the core of the work material was observed[6].

Attempts were also made to investigate the metal flow and contact condition[7] in each machine element, but the actual state of the deformation was hardly clarified because of lack of information. A strong need is therefore felt to take a new look at what is really happening when the rolling dies engage into a cylindrical workpiece.

Considering the four troubles above mentioned, the author has carried out a series of experimental studies, in which the features of the products were altered systematically. In the first place, cases of plain cylinders being rolled between flat dies are dealt with, and a detailed mechanism of plastic kneading common to all the components-rolling are fully clarified. Experimental results are supported by proposing a new type of consistent shear line field by which far advanced information in the components-rolling can be made available. In the next place, the forming procedure of a component having specific profile such as screw thread or gear tooth is treated. By comparing the actual deformation with the process models of rolling, points of importance in considering the process are revealed. To detect a three dimensional pattern of the material flow, the split plug, buried in the workpiece, has been employed. By examining a distorted grid of the plug, the constituent deformation occurring in the core portion of the specimens is revealed for the first time. Effect of this core distortion on formation of a

surface feature has been assertained to find some controlling factors of deformation throughout a rolling process. Thus, (1) phenomena common to all the components-rolling and (2) deformation characteristics in accordance with the individual feature of a product have been clarified respectively.

2. Some Aspects of Deformation in Components-rolling

Fig. 1 shows a circumferential distribution of effective diameters of a screw thread sold at a market which is ascertained by the two-wire method. Though this is merely an example, we can notice a peculiar configuration of the cross-sectional profile which is generally inherent in all the components-rolling. The more of additional revolutions of the workpiece are given, the closer the accuracy of roundness obtained may be, but an excessive rolling which brings about a crack in the core zone of the material as illustrated in Fig. 2 is a trouble.

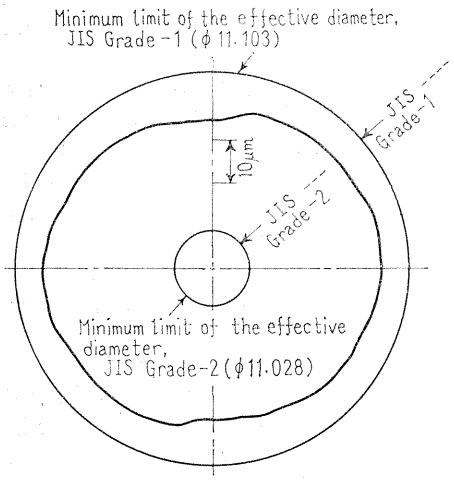

Fig. 1. Distribution of effective diameters of a rolled screw thread sold at a market.

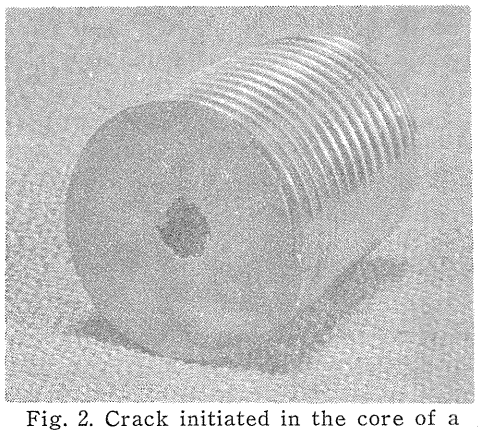

Fig. 2. Crack initiated in the core of a screw thread.

The photographs in Fig. 3 show the deformed grid-line patterns after rolling. The deformed pattern was originally 0.1 mm square and the grid was scribed on one parting plane of a flow-detective split plug which was previously built in the workpiece. This is a useful technique in the laboratory to visualize the deformation of anywhere throughout the material, the details of which are found later (see Chapter 5). In Fig. 3, (a) shows the cross section of a rolled blank with plain dies (a plain cylindrical component was aimed at.), (b) is also the cross section of a rolled screw thread, and (c) is that of a rolled spur gear. Curves in Fig. 4 show plots of the tangential displacement of each point on a radial line in Fig. 3. As will be seen in Fig. 3 and Fig. 4, the deformation patterns of the above three cases are mutually much alike in the core zone, but the conditions are somewhat

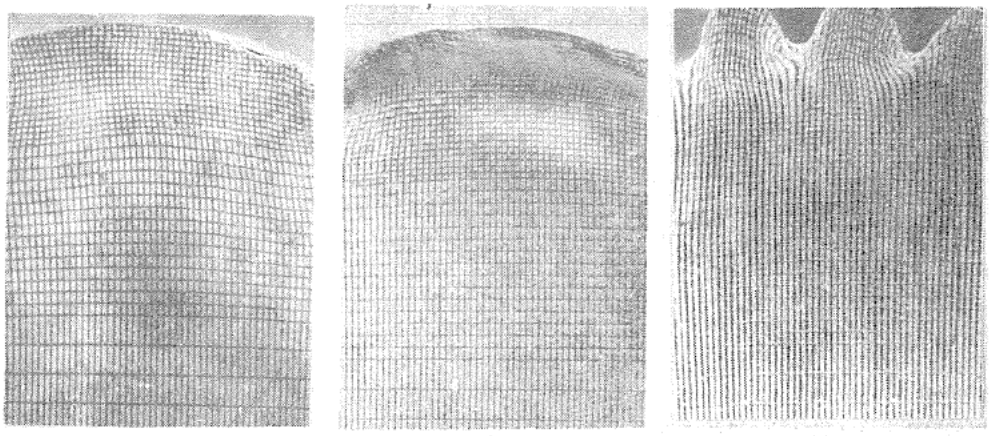

(a) (b) (c)

Fig. 3. Deformed grid-line patterns after rolling.
(a) Plain cylindrical component (reduction: 2%)
(b) Screw thread (root of a metric thread)
(c) Spur gear (pressure angle: 30°)

peculiar in the surface region because of the surface feature. In traditional treatments it was believed that in the thread rolling or gear rolling the principal part of the work material was left as a rigid core, but in reality, the distortion similar to that in Fig. 3 (a) prevails all over the cross section of the work material as shown in Fig. 4.

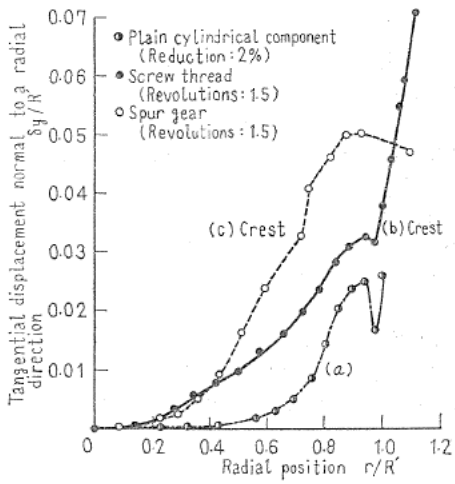

Fig. 4. Distortion of a radial-line in a cross section.

3. Plastic Kneading in the Rolling of Cylindrical Components[8]

3. 1. Introduction

To analize in more detail the process of the components-rolling, it is necessary to understand the plastic kneading which is seen in all the components-rolling. As the plastic kneading is realized most outstandingly in the Mannesmann piercing process, many studies have been made on this type of the forming process and some investigators[9] have proposed models of the deformation mechanics in rolling a cylinder. The analyses, however, seem to lack something in completeness; for

one thing, (1) they are independent of the rotation of the component on its axis, and (2) they are inconsistent in the deformation field throughout a cross section of the cylinder. The author proposed a prototype of a consistent shear line field[10] in 1971, and recently, K. Kato tried to calculate an approximate value of the stress by simplifying the author's solution[11]. M. Hayama attempted to estimate the loads and the contact widths in the lateral oblique upsetting of a cylinder using an upper bound solution with the rigid triangle velocity field[12]. The Hertzian contact of the material has been examined by J. E. Merwin and others[13].

The current chapter deals with the cases of plain cylinders being rolled between plain flat dies. Configuration and deformation of the material in rolling are clarified. By examining the normal and tangential components of a force acting on the die face with two kinds of specially equipped dies, the distribution of both components of stress has been newly estimated. Experimental results are supported by proposing a new type of shear line field according to which a far advanced information on the essentials of deformation can be made available.

3. 2. Method of experiment and conditions

The scope of this treatment is limited by the following conditions.

(1) Type of tool: flat dies

(2) Surface of die: plain die without any significant feature

(3) Rate of reduction: constant except the run-in period

So, the product obtained in this process is a cylinderlike component as shown in Fig. 3 (a) in which an extremity of deformation in the rolling is intended to test although a workshop never aims at this type of product.

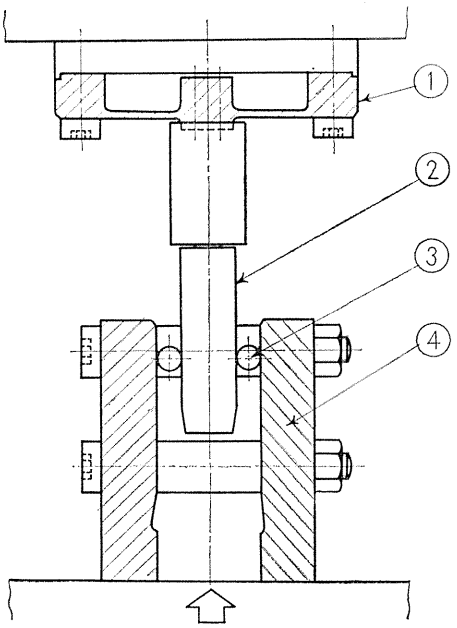

Fig. 5. Apparatus for the rolling of cylindrical component.

A sketch of the test rig is shown in Fig. 5. A flat central-die ② carried on a diaphragm ① was fixed to the upper part of an oil hydraulic under-drive press, and a pair of opposed-dies ④ was mounted on the moving table of the press. Two blank cylinders ③ are rolled symmetrically and the normal components of forces acting on the die faces are self-balanced. Previous to the rolling operation, blank cylinders were fixed at their starting-positions with a set of gauge blocks. In the experiment, two different types of central-die, which are shown in Fig. 6 and Fig. 7, have been also used.

The normal component of stress acting on the die face was measured by a pressure pin method. Details of the die with a pressure pin are given in Fig. 6. The driving force (total tangential component of force acting on the die face) was detected by wire strain gauges attached to the diaphragm ①. Distribution of the tangential stresses was obtained from a central segmental-die (Fig. 7) whose seg-

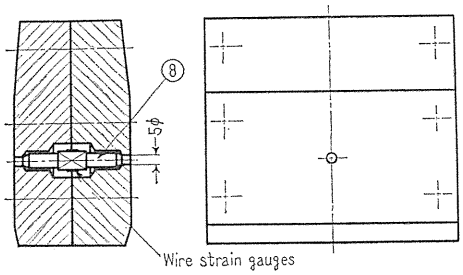

Fig. 6. Central die with a pressure pin.

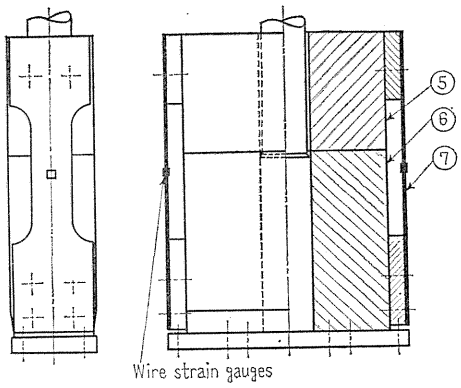

Fig. 7. Central segmental-die to measure the distribution of shear stresses.

ments, ⑤ and ⑥, were connected by two tension plates ⑦. Contact of the component with the die surface was on segment ⑥ at the early stage of the process, moving on to segment ⑤ as the process continues and a part of the tangential force on segment ⑤ gives a response through wire strain gauges on the tension plates ⑦. Relative displacement of the central-die to the opposed-dies was detected by a variable-inductance type transducer.

As a blank material, A1100F (JIS) commercially pure aluminium was used in the majority of the experiments and the stress-strain curve from a well-lubricated compression test is given in Fig. 8. Blank cylinders with a diameter d_0 of 18.85 mm and a length l_0 of 50 mm were machined from bars in the as-received condition. It has been made clear by experiment that the end effects were insignificant when $l_0/d_0>2.5$.

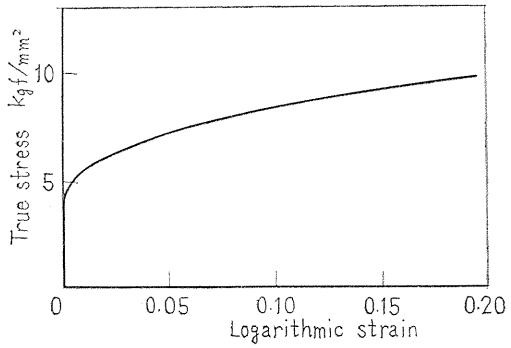

Fig. 8. Flow stress-strain curve for A1100 aluminium obtained from well lubricated compression test.

Reduction in the rolling, which is defined as {(original diameter of the blank) —(minimum diameter of the rolled component)}/(original diameter of the blank), was varied in the range of 0.5~2% and its variation was attained by inserting

spacing collars of different heights between the opposed-dies. The dies, the collars and the fastening bolts were designed to be sufficient in rigidity, and the inter-spaces between the central-die and the opposed-dies were inspected by using the gauge blocks.

Profiles of deformed components were measured by a toolmaker's microscope with a detective feeler and a precision angular dividing attachment.

The specifications of tools, material used, and the other experimental conditions are tabulated in Table 1.

Table 1. Experimental conditions (plastic kneading)

blank material	material : aluminium (A1100 BE)* 0.2% proof stress : 4.8 kgf/mm^2 strain hardening exponent : 0.2 diameter : 18.85 mm length : 50 mm
dies	material : S 55 C surface roughness : $R_{max}=4\mu m$ relative speed of two dies : 5.5 mm/sec
temperature	(20±1)℃
lubricant	not used
reduction	reduction $R=\{(D_0-D_{min})/D_0\}\times 100\%=(0.5\sim 2)\%$ D_0 : original diamater of the blank D_{min} : minimum diamater of the rolled component

* Lead was used in some experiments.

3. 3. Deformation of cylinders

Some of the specimens were cut into halves by a cross-sectional plane and grid lines were scribed on the one side. Then, two halves were reassembled by glueing with Araldite. The assembled total lengths of specimens are 100 mm and diameters

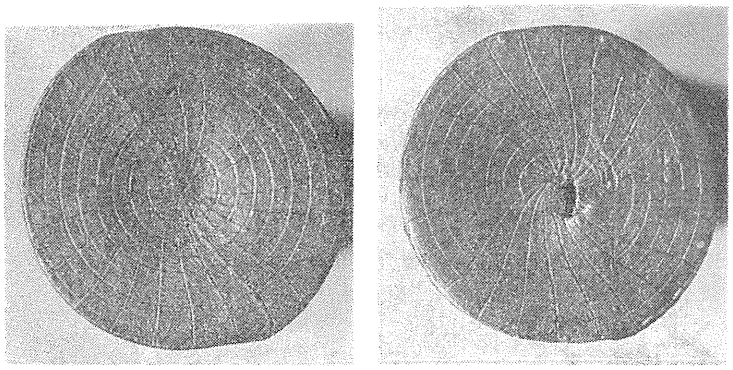

Fig. 9. Photographs of the distorted grids.
(a) reduction: 4.1%, revolutions (number of turns): 1.25, material: lead
(b) reduction: 3.4%, revolutions (number of turns): 1.5, material: lead

19.0 mm. Sample photograph of the distorted grids after initial 1.25 revolutions with a reduction of 4.1 % is shown in Fig. 9(a). Continuing the rolling with some larger reduction, a crack initiates near the central position of the specimen as in Fig. 9(b).

The deformation in this process is obviously different from that[14] in a lateral compression without rolling. Supposing that the process continues in a steady state, it was examined how the whole of the work material deformed plastically by superposing two same photographs which are slightly shifted in rotation. To meet the case, typical configuration of component might be drawn schematically as in Fig. 10. The whole component is distorted plastically with little axial extension and the contact region with the die is shifted toward the "inlet side" (A in Fig. 10).

There are three zones in the contact region: a small initial elastic zone, a plastic zone, and a zone of elastic recovery. In Fig. 11 are shown the whole

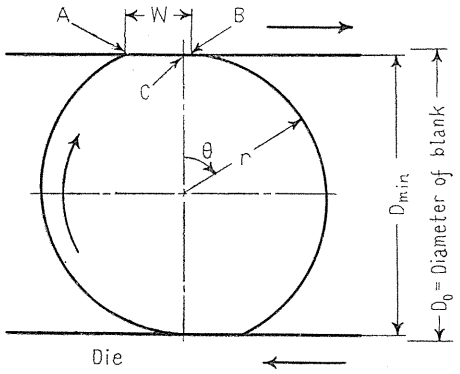

Fig. 10. Typical configuration of a cylindrical component in rolling.

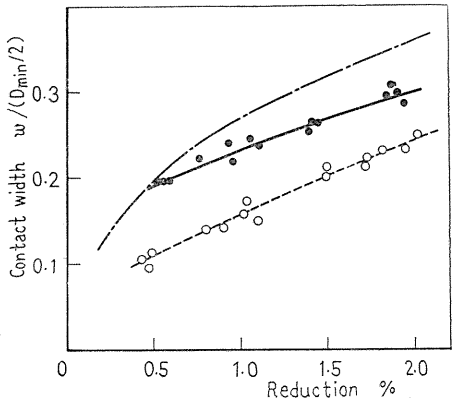

Fig. 11. Contact width of the components in rolling, after rolling and without rolling.
Solid line: contact width during rolling estimated from working period of a pressure pin.
Broken line: width of flattened region of the unloaded component after rolling
Cain line: width of flattened region of the laterally compressed component without rolling

contact widths for aluminium specimens (Table 1) expressed in terms of $w/(D_{min}/2)$. The solid line is the contact width during rolling estimated from working period of a pressure pin, and the broken line is the width of flattened region of the unloaded component. The former is larger than the latter by 3~5 % of the blank diameter and the specific difference between two curves, which suggests the elastic recovery, is relatively large for low reductions. In comparison with the lateral compression test without rolling, the flattened region of the case without rolling, shown by a chain line in Fig. 11, is larger than that with rolling (broken

line in Fig. 11) by 5~7 % of the blank diameter. It will be evident that there exists a drastic difference in deformation mechanism between the rolling and the lateral compression without rolling.

Profiles of components under steadily deforming condition are shown in Fig. 12. Notations in this figure correspond to those in Fig. 10. Radius r changes in succession, and its variation is most remarkable at the contact region A–B. The position where the radius r attains the minimum value should be right over the center of component (C in Fig. 10).

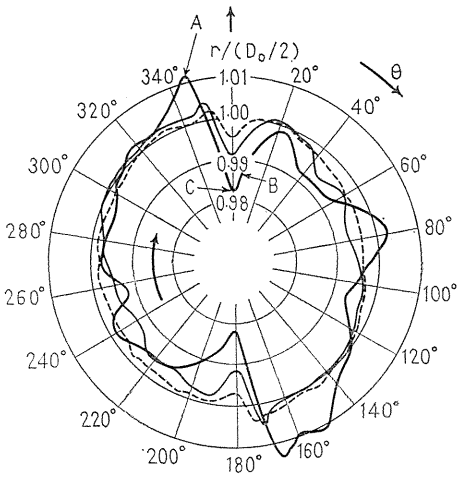

	Reduction	Revolution
———	1.82 %	0.86
———	0.91 %	1.08
-----	0.43 %	1.03

Fig. 12. Measured profiles of components.

3. 4. Forces and stresses acting on the contact region

The tangential driving force against revolutions of cylinder (die travel) curve obtained in rolling an aluminium specimen with a reduction of 1.1 % is given in Fig. 13. Tangential driving force takes its maximum value at the stage after an

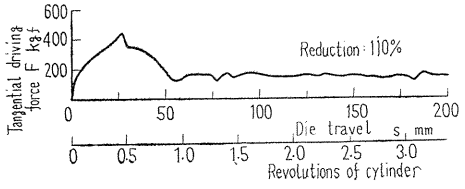

Fig. 13. Curve of tangential driving force against revolutions of cylinder and relative die travel.

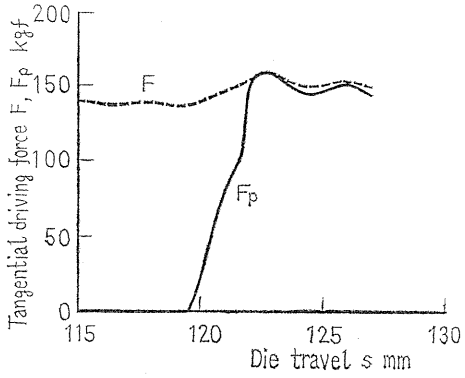

Fig. 14. Total tangential driving force and a part of tangential force acting on segment ⑤.

initial half-revolution of the component and seems to keep a steady value after it makes one revolution. In a steady state rolling, the total tangential force F and a part of the tangential force Fp acting on the segment ⑤ in Fig. 7 were recorded as in Fig. 14.

A response of the pressure pin to the normal component of force is shown in Fig. 15. The pressure records were taken in various positions of the die and it was observed that a rather moderate change of normal force also occurred at the early stage of the process.

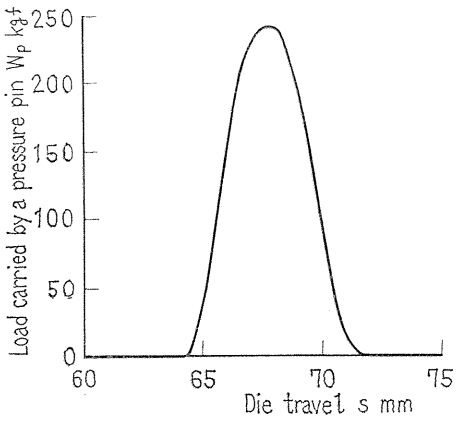

Fig. 15. Response of a pressure pin to the normal component of force.

From the records obtained as above, the distributions of the normal and tangential components of stress were estimated as follows: The contact zone of a component, when its width is smaller than the diameter of the pressure pin, extends across the face of the pressure pin. Accordingly, the output of the pressure pin (Fig. 15) can reflect not only the distribution of the normal components of stress but also the area of a contact zone at the relevant instant. Having recource to this fact, the distribution of the normal stresses can be estimated by a progressive calculation (see Appendix). The distribution of the tangential stresses is computed from the gradient of the load against die travel curve recorded by means of the central segmental-die (Fig. 14).

Fig. 16 shows the distribution of both components of stress at a steady state obtained by above techniques. In this figure, the normal components represent the negative values of the stress. The pressure is larger at the inlet side than at the receding side, but its distribution is rather moderate in undulation. On the other hand, the shear stress distribution shows an inexpected tendency. In the case of a large reduction, distribution curve of the shear stress has a strong peak at a receding side. With a decrease of the reduction, the peak diminishes gradually, and the shear action becomes more serious rather at the inlet side. Since the proof stress of the material is 4.8 kgf/mm², it seems that on the whole a rather high pressure is introduced in the contact region and a sufficient interfacial shear stress is generated at the receding side to revolve the material.

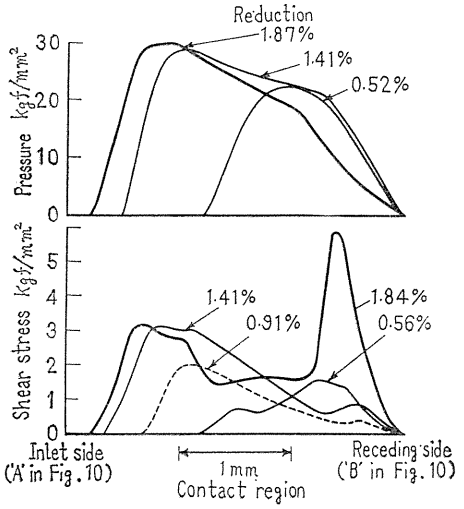

Fig. 16. Distributions of the normal and tangential components of stress in the contact region.

For the steady state, the mean va-

lues of the pressure and the shear stress are plotted against the reduction in Fig. 17. Though a change in the reduction influences the mean shear stress to a significant extent, one might expect that the mean pressure would scarcely reflect the rolling condition.

Referring to Fig. 17, the ratio of the mean shearing stress $\bar{\tau}$ to the mean pressure $\bar{p}$ will be easily calculated, the result of which is shown in Fig. 18. In the figure the ratio of contact width to minimum diameter of the rolled component w/D_{min} is shown for comparison. It will be seen that the $\bar{\tau}/\bar{p}$ values give a trend similar to the w/D_{min} curve which states approximately the static equilibrium of the moments due to the external forces.

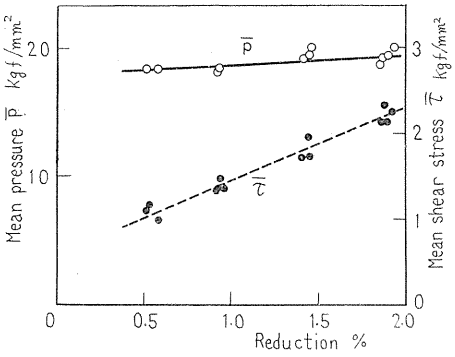

Fig. 17. Mean values of the pressure and the shear stress in the contact region.

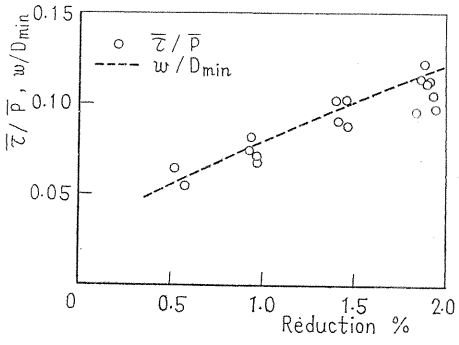

Fig. 18. Ratio of the mean shearing stress to the mean pressure and ratio of the contact width to the minimum diameter of the rolled component.

3. 5. *Proposal of a shear line field*

The deformed grid pattern in Fig. 9 reveals a final distortion of the component, but it appears impossible to state where the largest strain rate occurs and in what

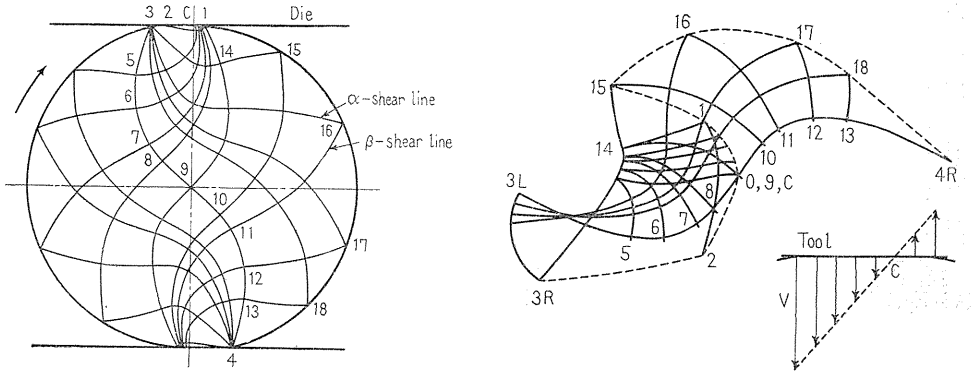

(a) Shear line field. (b) Hodograph.

Fig. 19. A shear line field compatible.

direction the metal particles flow. Supposing that the process continues in a steady state, a displacement vector diagram is yielded by superposing two same photographs which are slightly shifted in rotation. Referring to the approximate instantaneous velocities and the stresses described, the author proposes a consistent shear line field for a plane plastic deformation of a plastic-rigid body as in Fig. 19. The relative rotative movement of die and the equilibrium of moments are taken into consideration to construct the shear line field throughout a cross section of the work material.

3. 6. Summary

The investigation reveals a detailed mechanism of the plastic kneading which is observed when a plain cylinder is rolled between the plain flat dies. On the basis of this experimental study, fundamental phenomena common to all the components-rolling have been fully clarified.

The results obtained are summarized as follows:

(1) The deformation process which takes place in rolling a cylindrical component is quite dissimilar to that in a lateral compression without rolling. The whole work material deforms plastically presenting a particular configuration of the cross sectional profile which is generally inherent in all the components-rolling.

(2) There are three zones in the contact region, namely, a small initial elastic zone at the inlet side, a plastic zone extending to the receding side, and a zone of elastic recovery.

(3) The normal and tangential components of a force acting on die face were examined by experiment with two specially equipped dies, and the tangential stress shows a somewhat unexpected tendency which suggests a deformation mechanism particular to the comonents-rolling.

(4) The $\bar{\tau}/\bar{p}$ values coincide with the w/D_{min} value which is determined by the geometry of the contact. When the $\bar{\tau}/\bar{p}$ value does not follow the w/D_{min} value, the rolling will be impossible because of the slipping.

(5) Experimental results were supported by proposing a new type of consistent shear line field by which far advanced information on the essentials of deformation in the components-rolling can be made available.

4. Profile-shaping Process in the Rolling of Some Rotational Components Having Functional Features such as Screws and Gears[15]

4. 1. Introduction

In Chapter 3, cases of plain cylinders being rolled between plain flat dies were dealt with, and fundamental phenomena observed commonly to all the components-rolling were fully clarified.

In this chapter, the forming procedure of a component having specific profile such as screw thread or gear teeth will be treated.

First, a method of composing a deformation model of rolling will be proposed to give a criterion for the actual deformation. The composition is originally based on some simple accepted assumptions which are plausible. By comparing the actual deformation with this model, points of importance in considering the process were revealed. A point worth notice is a peculiar distortion common to the rolling.

When such a distortion is once brought about in the cross sectional figure, it will be retained and brought eventually into the finished parts. This chapter deals principally with the influence of this distortion on the forming mechanism of the profile features such as screw thread and gear teeth. Though, in this research, specimens for screw or for gear do not give exactly the form of a male screw or of a spur gear, hereafter they will be referred to simply as "the screw" or as "the gear", and their specific profile portions will be inclusively represented by a term "feature".

4. 2. Method of experiment and conditions

A sketch of the test rig is shown in Fig. 20. Rolling method is the same as the one in Chapter 3 in which two blank cylinders were rolled simultaneously. This time, however, the pressure-pin method formerly employed for measuring die pressure should be abandoned because of the specific profile of the workpiece. So, it was decided to detect the normal component of force acting on the die face by the wire strain gauges attached on the tie-rods. In spite of the evident ability of this testing device, details of the load measuring system as well as the examination of the rolling force will be left to the next chapter.

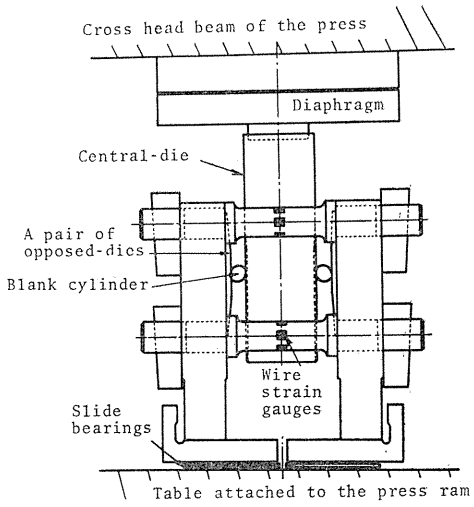

Fig. 20. Tool arrangement for components-rolling.

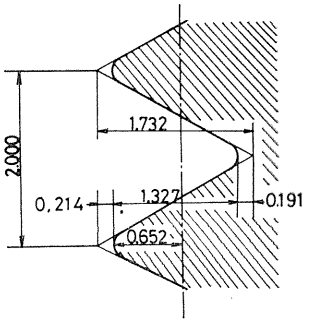

Fig. 21. The profile feature of the dies.

Two pairs of forming dies are provided with a profile feature of triangular ridges which are common to both the screw and the gear except the lead angle of 0° in the former in contrast with 90° in the latter. The cross section of the dies' feature has an old standard form of metric thread of a 2 mm pitch as shown in Fig. 21.

The specifications of tools, material used, and the other conditions are tabulated in Table 2.

Fig. 22 shows the details of inlet part of the die whose proportion is in accord with the practice in the production line. This inlet ramp of the working face of

Table 2. Experimental conditions (components-rolling)

dies	flat dies for the screw lead angle : $\beta=0°$, pitch : 2 mm	flat dies for the gear lead angle : $\beta=90°$, pitch : 2 mm pressure angle : 30°
blank sizes	diameter : 16.52 mm length : 50 mm	diameter : 16.68 mm length : 50mm
blank material	aluminium A1050F	aluminium A1050F
products	screw-like component effective diameter : 16.438 mm	gear-like component diameter of pitch circle : 16.553 mm
other conditions	lubricant : not used rolling speed : 5.3 mm/s temperature : (20±1)℃	lubricant : not used rolling speed : 5.3 mm/s temperature : (20±1)℃

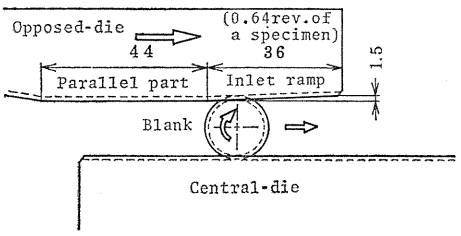

Fig. 22. Details of the inlet part of die.

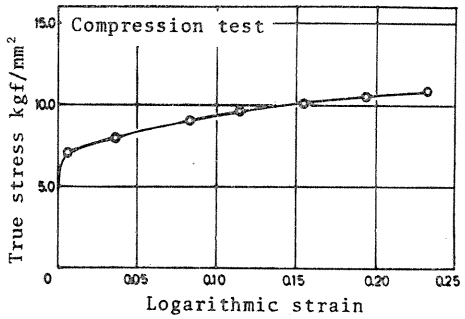

Fig. 23. Flow stress-strain curve for A1050F aluminium.

the outside dies determines the amount of die penetration per each half revolution of the blank. In this case, the inlet ramp can give a revolution of 0.64 before the workpiece reaches the parallel portion of the die. Therefore, the specimen as a whole completes a full reduction after revolving an amount of 1.14, as this ultimate reduction is given by a constant clearance between parallel parts of dies. For this reason, only the phenomena during initial 1.5 revolutions will be described in this chapter. though 5 to 7 revolutions are generally needed for completion of a practical process.

Specimens are cut from commercially pure aluminium bars of the specification A1050F (proof stress=6.69 kgf/mm²), their stress-strain curve by a well-lubricated compression test is given in Fig. 23.

Profiles of deformed components were measured by a tool-makers' microscope with a precision angular dividing attachment and a tracer-type form tester, and deviations of the equivalent effective diameters of a half-rolled product from the final effective diameter aimed at were measured by a floating micrometer with two appropriate cylinders.

4. 3. Configuration of workpieces in rolling

Fig. 24 (a) shows circumferential distributions of effective diameters measured

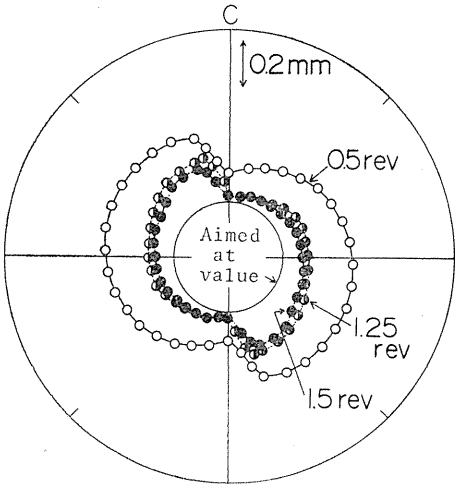

Fig. 24. (a) Peripheral distribution of effective diameters in the screw.

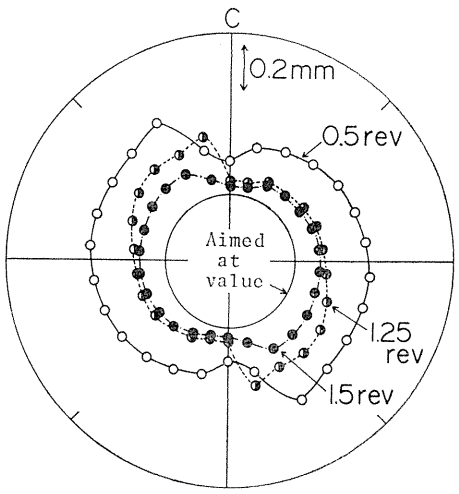

(b) Peripheral distribution of pitch diameters in the gear.

along a groove generated in the screw by two-wire method. Since the curves in this figure represent merely deviations from the final value of an ideal effective diameter, the realistic configuration typical of rolling should be the one schematically illustrated in Fig. 25. It appears to have something in common with the cross sections of plain cylinders being rolled between flat dies as shown in Chapter 3. Though a deviation in effective diameters decreases with the number of turns, a roundness deviation in effective diameter stands at more than 0.2 mm even after initial 1.5 revolutions*.

Fig. 24 (b) shows deviations in the pitch diameter of the gear, which are measured by the over-pin method. These deviations seem to be the same in nature as those in effective diameter.

In order to have the circumferential profile on the whole in the screw, a workpiece rolled halfway was taken out and mounted between centers of a circular dividing attachment of toolmakers' microscope. Thus the diameters of the root and the crest at any peripheral position could be measured by means of the stage

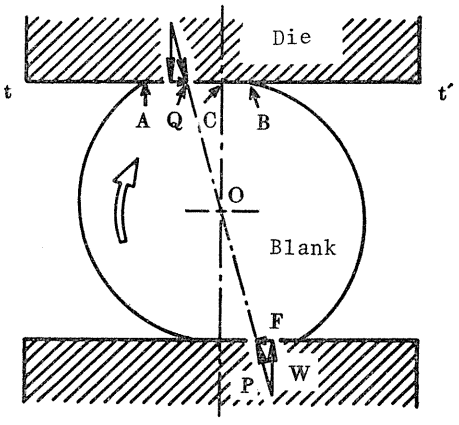

CO : Center of the bite

Fig. 25. General material configuration typical of the components-rolling.

* As would be seen in Fig. 1, we could notice also such a peculiar configuration of the cross-sectional profile of a screw thread sold in the market, in which the number of turns seemes to be 6~7 rev..

micrometer of the microscope. The results obtained at three stages can be plotted as shown in Fig. 26. Deviations of the root diameters (black points) from a circle are evident with consequent variation in the height of thread (radial distance from a white point to a black one).

In the case of the gear, the halfway-rolled workpiece was mounted directly on the stage-glass of the microscope so that its axis coincided with the rotating axis of the stage. Points in Fig. 27 represent circumferential traces of tips and roots of the gear. By comparison of these figures, the gear appears to decrease the irregularity of its cylindrical form more in the earlier stage of revolution than the screw.

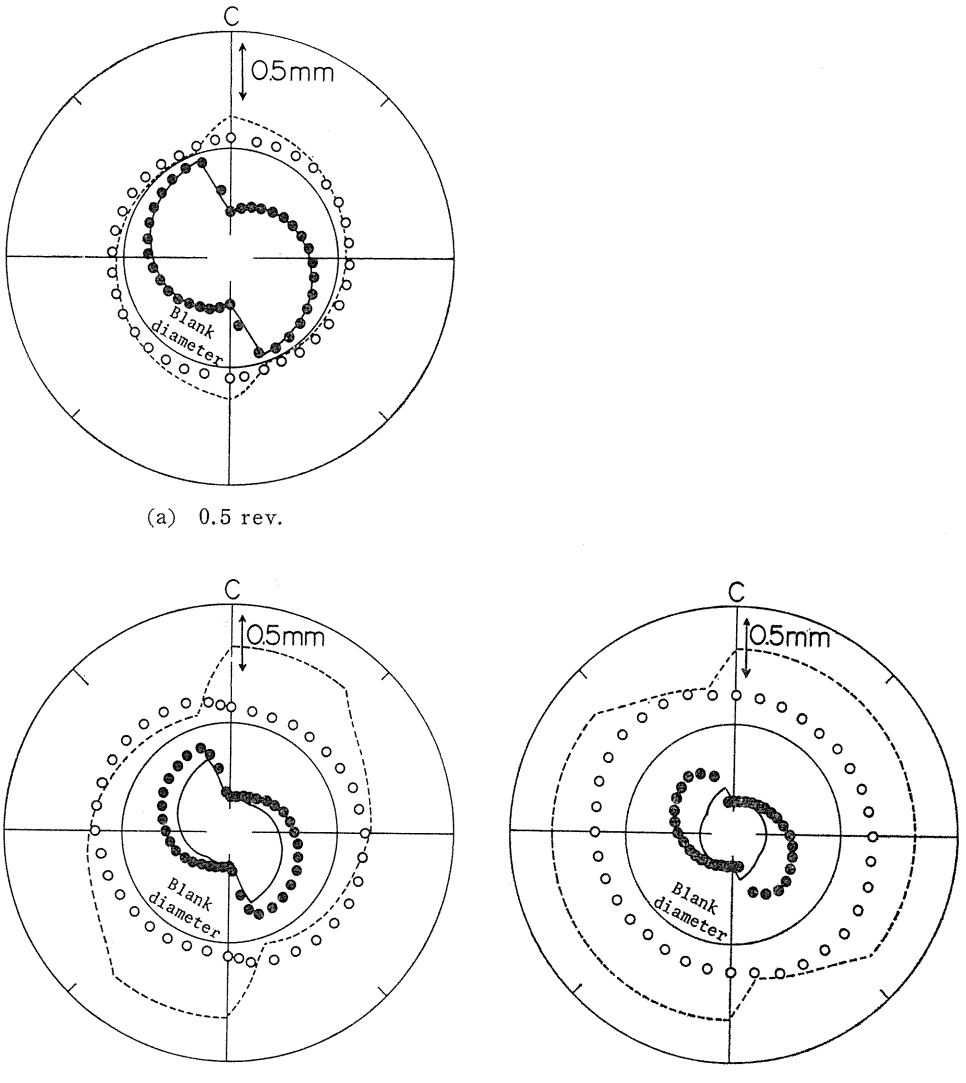

(a) 0.5 rev.

(b) 0.75 rev.

(c) 1.0 rev.

Fig. 26. Peripheral distribution of minor and major diameters in the screw.

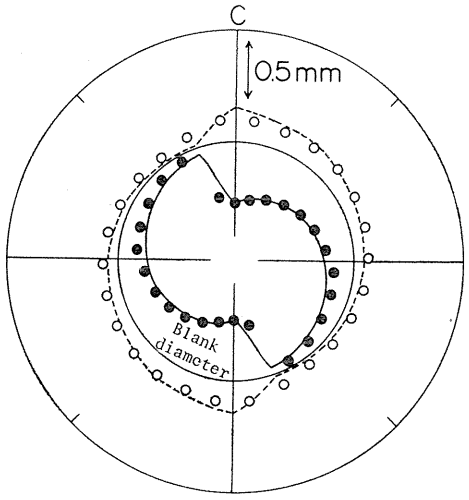

(a) 0.5 rev.

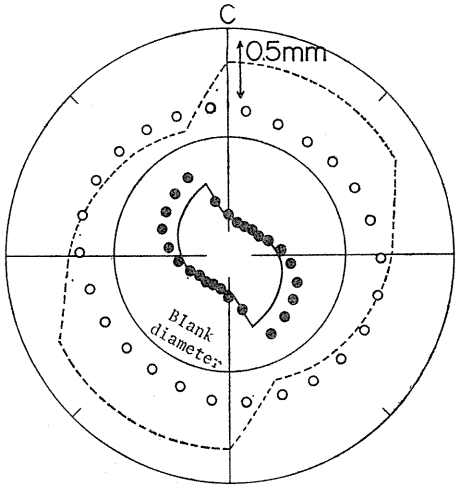

(b) 0.75 rev.

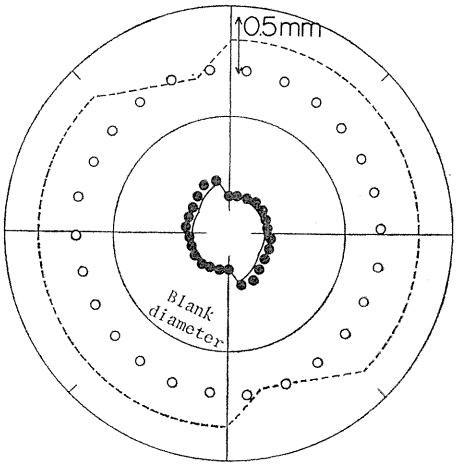

(c) 1.0 rev.

Fig. 27. Peripheral distribution of root and tip cylinders in the gear.

4. 4. Process of die penetration in the components-rolling

In the components-rolling, the specimen undergoes die penetration in a quite different manner from that seen in the strip rolling or other continuous processes. It is important in studying the mechanics and metal flow of a blank to realize the condition of die penetration and its effects on each point of a specimen. As the dies shown in Fig. 22 bite into a blank cylinder and the rolling goes on, the bitten portions of material should suffer a nominal reduction in diameter along a straight envelope line OPQ in Fig. 28 where the line OP corresponds to the inlet ramp of the die and PQ to the parallel portion in Fig. 22. Fig. 29 shows the spatial identification of a cylinder referring to which the position of the specimen at a rolling

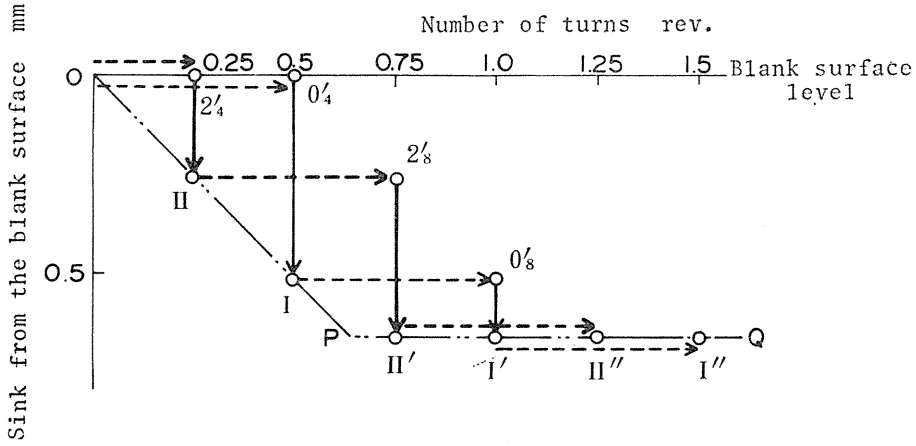

Fig. 28. Die penetration and corresponding passage of rolling which each point followed.

stage is considered. The bitten portions of material are indicated by 0 and 4, and other intermediate portions are identified by adaptable numbers. Refferring to this positional notation, the point 0' fixed on the material, for example, situated on 0 at the initial stage should undergo a first reduction $0'_4$ I (in Fig. 28) at point 4 after an initial rev. of 0.5, and a second reduction $0'_8$ I' at point 8 after a total rev. of 1.0. On the other hand, material point 2', which starts from a position 2, undergoes a first reduction $2'_4$ II at point 4 after an initial rev. of 0.25, and a second reduction $2'_8$ II' after a total rev. of 0.75 In this manner, at every half revolution the material undergoes a different incremental amount of die penetration according to its peripheral position occupied when the rolling starts. Thus the amounts of incremental reduction and their imposing stage vary considerably, though the amount of final penetration (PQ) should be equal for all the material points. It is essential to understanding the components-rolling to realize the variety of this deformation career distributed along the periphery of the specimen.

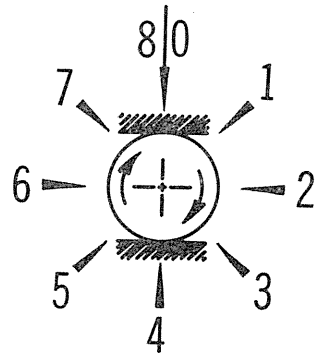

Fig. 29. Spatial identification of a cylinder.

4. 5. Composition of the deformation models

Though the distortion of a cross section shown in Fig. 26 and Fig. 27 tells an aspect of deformation in its own way, a more detailed character of the process will be elucidated by visualizing the "process models of forming" and comparing them with the experimentals. A process model for the screw can be constructed on the basis of the condition of volume constancy and some simple assumptions as follows.

(1) Total length of a specimen does not change throughout the process. Accordingly, a radius which passes through a crest or a bottom of the thread does not move in axial direction.

(2) A meridian plane remains a plane during the process.

(3) Die penetration causes a piling up of the thread ridges so as to compensate just the volume of sinking in the contact region. Unconstrained surface which is free from tools (for example, 1, 2, 3 in Fig. 29) remains as rolled, its radius being the same as OB in Fig. 25. In other words, the core of the specimen can not deform plastically.

(4) In profile of the meridian section at any intermediate stage, the crest assumes a plateau constructed by an axial-parallel line.

Assumption (3) is, among others, very influential in description of the deformation pattern and in estimating the forces required, as will be found in the next chapter.

Fig. 30 shows plots of the calculated major and minor diameters of the screw at three stages in a process. "Distortions in cross section due to die penetration" are well seen in these curves, but this type of distortion should disappear after initial 1.14 revolutions in this process model.

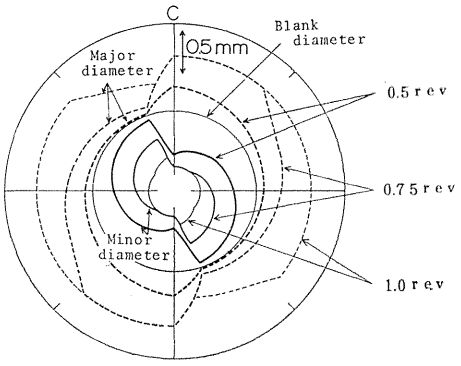

Fig. 30. Process models of the screw.

On the other hand, process models for the gear are constructed on the following assumptions.

(1) Total length of a specimen does not change throughout the process.

(2) A meridian plane of symmetry which passes middle of a tooth width or a space width remains a plane during a process.

(3) Central angle between the neighbouring meridian planes mentioned above keeps a constant value, and the tool engages with involute tooth form of the specimen properly.

(4) Tip surface of the tooth piles up in the space of the die profile retaining a cylindrical form.

In fact, the calculated values of piling up under a constant penetration of dies showed little difference between the screw and the gear.

4. 6. Comparison of the experimental process with the model, and discussion

As the model might be supposed to give a copy-book deformation, by comparison of the experimentals with this model we can easily get an idea of how unexpectedly a real material behaves.

Turning to Fig. 26 again, two kinked fine lines show the circumferential root and crest lines by the model drawn to make a comparison with the experimentals, where the full line represents the root and the broken line the crest. It will be seen that the agreement in the root diameter, between black points and full lines, is fairly good at the initial stage of 0.5 rev. (Fig. 26 (a)). As the rolling goes

on, however, the actual root diameter becomes far larger than the model diameter except at the center of bite C as will be seen in Fig. 26 (b). Since a penetration is always accompanied by a lateral expansion of the core as a whole, the experimental root diameter shown in Fig. 26 (c) becomes considerably larger than the models', Moreover, the actual height of threads obtained is shorter on the whole than the models' except in certain portions in (a). According to the model the crest should pile up rapidly near the bite center due to the rapid sinking at the root, but the actual piling up is quite moderate. So, undoubtedly some of the assumptions in section *4. 5.*, so far accepted by many investigators in considering the deformation mechanics of components-rolling, cannot be said to hold for further analyses.

An examination of three dimensional pattern of the metal flow in the specimens and its effects on the forces required will be described in the next chapter. Here, in view of only the deformation some comments on the assumptions will be given in brief.

Assumption (1) is said to be practically correct: the reason will be shown in Chapter 5 where the so called 'split plug' method is applied for detailed strain analysis.

Assumption (2) is incorrect in the strict sense as will be seen in Fig. 3 (b) and Fig. 4, but even when the distortion of the meridian plane exists to some degree, it is thought that this distortion will scarcely affect the behavior of piling up of the thread ridges. The form tester record gave such a profile curve at the bitten portion of a cross section through a root as in Fig. 31, and it is evident that no bulging at the inlet side did occur.

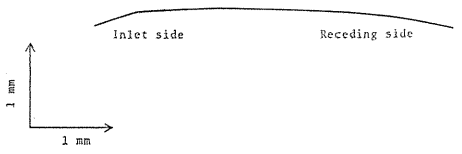

Fig. 31. Profile curve at the bitten portion of a cross section through a root of a screw.

Assumption (3) is unrealistic, because the difference between the observations and the process models will never be understood unless we assume that the material undergoes plastic deformation as a whole. As will be shown later, feature-formation component of a penetration, which can be estimated by subtracting core distortion component from an apparent penetration, should be applied to the process models.

Assumption (4) is correct except at the initial stage of the rolling. Fig. 32 shows a stereo-graphical view of a thread profile recorded by a form tester, in which we can see a localized piling-up at the beginning stage of bite, and this would bring about an under-estimatiton of the major diameter by the process model shown in Fig. 26(a).

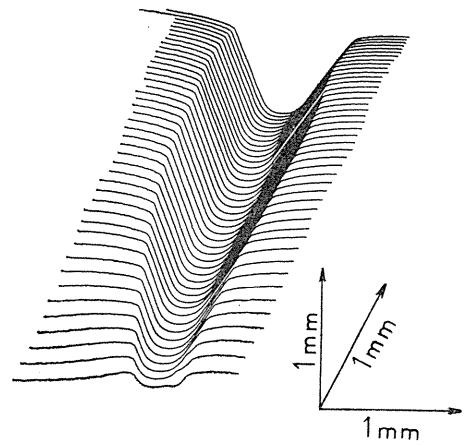

Fig. 32. Stereo-graphical view of a thread profile.

Fig. 27 gives similar analyses on the

gear**. In the gear, though the general tendency was similar to the screw, the observed root cylinder came closer to the model in Fig. (c). The tip cylinder observed was smaller than the model. Comparison of the gear tooth forms between the ideal and an observed one is made in Fig. 33. As will be seen from Fig. 27 and Fig. 33, in case of the gear not onty the assumption (3) but also (4) seems incorrect.

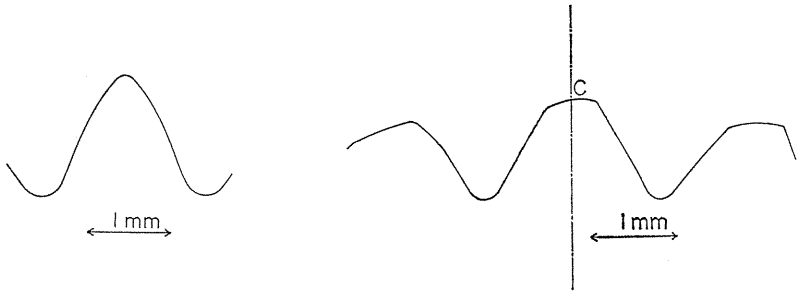

(a) Ideal form (b) Observed form (1.25 rev.)

Fig. 33. Gear tooth forms.

Referring to Fig. 26 and 27, we can see how the height of the thread or the tooth grows with the number of turns. Fig. 34 gives this development by so to say the feature-forming-ratio $\phi=h/h_f$ against the number of turns of component, where h is the current height of a thread or of a tooth, and h_f the final must-

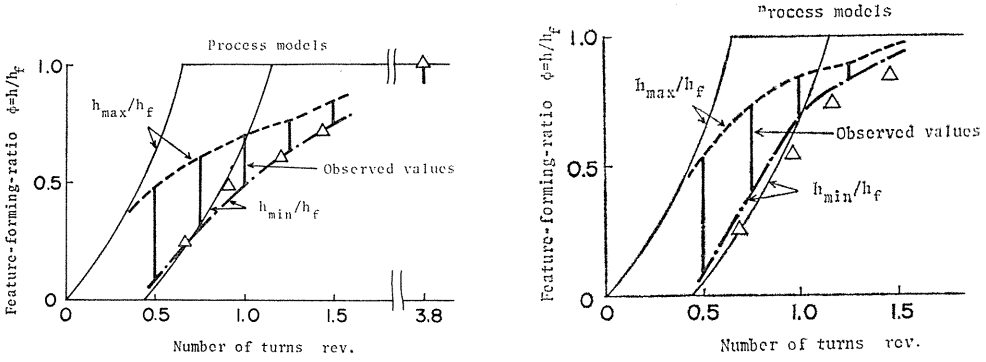

(a) Screw (b) Gear

Fig. 34. Feature-forming-ratio.

height. As illustrated in Fig. 35, the h values, both in the process models and the observed results, vary with the circumferential position. Thus, the feature-forming-ratios observed should be represented for ranges between h_{max}/h_f and h_{min}/h_f as vertical lines shown in Fig. 34. In the case of the screw (Fig. (a)), as well

** In the experiment on the gear, die working space was set a little narrower than the nominal value intentionally.

as the gear (Fig. (b)), observed feature-forming-ratios appear to develop fairly more slowly than those of the process models, and this suggests that the central core of the components deforms plastically so as to have a share of the die penetration.

Supposing that Fig. 35 shows the cross-sectional configuration of the screw when it has made a number of turns of 0.75, the material points C′ and C″ are just passing through a spatially fixed point 0 in Fig. 29, and the points A′ ane A″ are beginning to contact with a die at the inlet side. Tracking these material points from the beginning of the process, current major and minor diameters corresponding to these points were measured. The results are shown by plots in Fig. 36. (a) gives an aspect of the actual die penetration into a material in the case of the screw which was assumed to take an ideal form of $2_4'$ II $2_8'$ II″ in Fig. 28. It should be noted that the diameters really increase for periods of 2 to 3 and 4 to 5 and so on. If we pay attention to the poiot of 0.75 rev., then we see that h_{max} is represented by the ordinate difference of C_4' C_4'' and h_{min} is given by that of A_3' A_3''. Turning our eyes on another material point of the same specimen, for example 0 $0_4'$ I $0_8'$ I′ in Fig. 28, we can see the actual passage of rolling as illustrated in Fig. 36 (b).

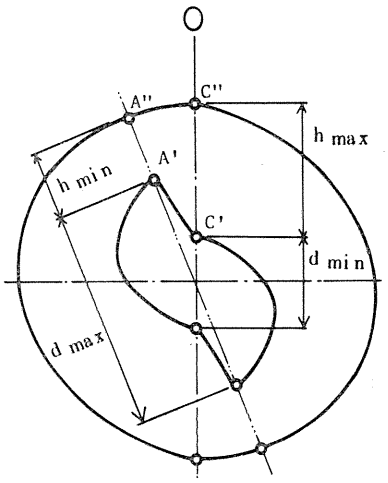

Fig. 35. Specification of the typical profile.

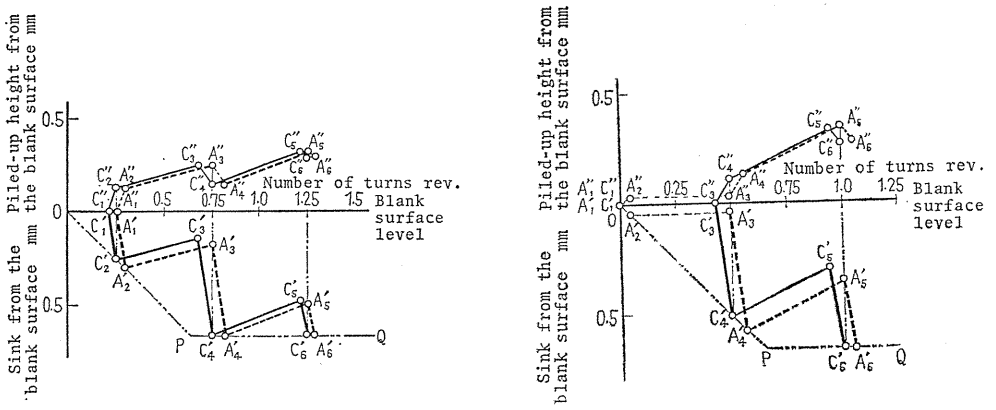

Fig. 36. Actual rolling passage of some points on a specimen (screw).
(a) Material point situated on the position 2 or 6 in Fig. 29 at the initial stage.
(b) Material point started from the position 0 or 4 in Fig. 29.

According to Fig. 35, a radial length of C′ C″ which gives h_{max} at 0.75 rev. should become h_{min} after about 0.47 rev. when the situation becomes similar to A′ A″ of the beginning of bite. But, if we assume that a height of the feature once attained does not change during the free revolution of about 0.5 after leaving the die, we can regard h_{max} of about half a rev. before the referred stage as h_{min} at that stage. Points denoted by △ (mark) in Fig. 34 are thus plotted as guessed h_{min}'s. It will be seen in the figure that, in the screw, guessed points almost lie on the h_{min}/h_f curve, but, in the gear, they are somewhat smaller than the observed values. In the latter case, it was observed that the rolling action to generate a tooth form was still effective in the receding side and this brought about a certain increase of the diameter.

Fig. 37 shows the distortion of the core by the ratio d_{max}/d_{min} of the maximum and the minimum of the root diameters. In the case of the screw (a), distortion observed is far larger than that expected from the process models, and a distortion once brought about in the cross section is difficult to vanish completely and it is brought eventually into the finished parts. In the case of the gear (b), a distortion observed seems to be similar to one of the process models, but the plastic kneading action in the tooth itself or around the root, as would be seen in Fig. 3 (c) in Chapter 3, will cause troublesome problems.

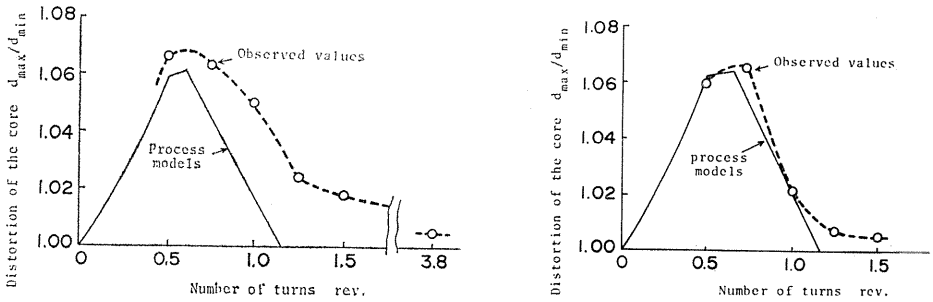

(a) Screw (b) Gear

Fig. 37. Distortion of the core.

4. 7. Summary

By means of experimental rolling of screw-like and gear-like components with profiled straight dies, shapes which blank cylinders come to develop in a process were observed in detail and processes of forming their functional features were fully examined.

The results obtained are summarized as follows:

(1) In the components-rolling, the process of the die penetration into a specimen is quite different from those seen in the strip rolling or other continuous processes. It is important to realize that the career of deformation varies from point to point in a specimen.

(2) Process models of rolling were proposed on the basis of some simple assumptions. Observed results did not agree with those process models except at

the initial stage of rolling, and this fact told us that the whole work material was really subjected to plastic deformation. Plastic deformation in the core part of the specimen appears to have considerable influence on the forming of profile features. Such being the case, the process models requires some corrections as will be shown in the next chapter.

(3) Distorted figure in the cross section is brought into the finished parts and it seems to limit the accuracy of the products.

(4) Even though the occurrence of deformation in the core part delays the piling up of the feature to some degree, it brings about a more effective die penetration in the subsequent stage of rolling. So, even in the stage of smooth-out-rolling the feature continues to pile up, which phenomenon was more remarkable in the case of the screw. On the results of this chapter, deformation and the rolling forces will be analyzed in the next chapter.

5. Analysis of the Rolling Process[16)]

5. 1. Introduction

As described in Chapter 4, plastic deformation in the core part of the specimen appears to have considerable influence on the forming of profile features. Continued from the preceding research, rolling experiments were carried out on the screw-like and gear-like components to discriminate the core distortion component from the feature formation component. In particular, the author applied the split plug to an analysis of a three dimensional flow taking place in the material. Having recourse to this plug makes it possible to attain a consistent understanding of the phenomena encountered on the process and clarify the plastic flow which really occurs in the specimens.

It would be worth mention that by this analysis the constituent deformation occurring in the core portion of the specimens has been revealed for the first time. Effect of this core distortion on formation of the surface features has been ascertained and the controlling factors of compatibility of the core distortion and the feature formation are clarified. In this way, the mechanics inherent in the components-rolling has been visualized.

5. 2. Method of experiment and conditions

Experimental rolling device utilized is the same as the one shown in Fig. 20. Two flat dies facing each other move upwards relative to a central fixed die and two test specimens are rolled simultaneously. The tangential force is measured by resistance strain gauges attached to a diaphragm which is connected to the central die. The normal force is caught by those attached to four pillars connecting opposed dies which are laid on the moving table of an oil hydraulic press through flat caged needle roller bearings.

Accorcing to the caribration of the normal force, it was found that the interference caused by the tangential force was less than 2.5% and the maximum elastic receding of opposed dies was less than 7 μm.

The profile of dies was characterized by a standard metric thread of 2 mm pitch, lead angles of which are 0° in the screw and 90° in the gear. The material is aluminium A1050F bar of about 16.5mm in diameter, its proof stress being

6.69 kgf/mm² and the strain hardening exponent 0.18 (see Fig. 23). With regard to the experimental conditions, refer to Table 2 in Chapter 4.

5. 3. Detector of deformation, the split plug

The split plug ao called here is a small cylinder turned from an aluminium bar of the same material as the test specimen so as to make the workpiece material uniform as a whole when it is buried diametrically in a specimen.

The plug, 6mm in diameter, is split into halves by one meridian plane and on one of the parting planes square grid lines of 0.1 mm space are scribed with a diamond needle. Fitting scheme of the plug is shown in Fig. 38.

In experiment, after a prescribed number of turns of the specimen the plug was removed from it and the grid points were examined by viewing the sectional plane by a universal measuring projector. Their coordinates were read by a stage micrometer. The whole image of the section on the screen could be photographed for a general analysis of deformation.

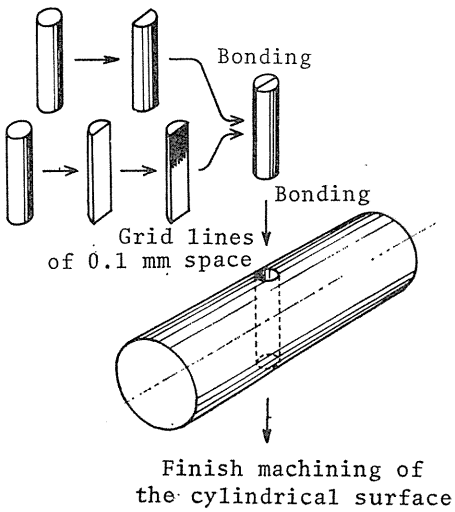

Fig. 38. Fitting scheme of the split plug.

As described in Chapter 4 the deformation history which a material portion in a specimen experiences is different according to the peripheral position occupied when the working starts with an initial bite. These initial positions have been identified by numbers 0 to 8 as shown in Fig. 29. The plugs could be so located that its axis coincides with any particular initial position, its sectional plane coinciding with a cross sectional plan of the specimen or a meridian plane. Here the initial positions and their working paths corresponding to only 0—4 and 2—6 axes will be treated identifying each by the path I and the path II as will be seen in Table 3.

5. 4. Observation of the movement of grid points according to the split plug

The notations a to h and b' to i' in Table 3 indicate respectively the length of path in I and II. Here, in order to represent the movement of a point an orthogonal system of coordinates is adopted as shown by (a) in Fig. 39 in which Oz corresponds to the specimen axis and Ox is so fixed that this line coincides with the central grid line of the plug after a prescribed rotation. Oy is perpendicular to Oz and Ox. Thus the displacement components in x, y directions are denoted by δ_x and δ_y. In axial direction, the strain was detected referring to a grid space of 0.4 mm and denoted by $\Delta l_z/l_z$ (see Fig. 39(b)). Fig. 40 shows by an example how the grid buried in a gear blank deforms after a revolution of 1.375. Fig. 41 shows how points on the central line move radially after various rotations, in which the ordinate means a specific movement relative to the current root

Teble 3 The initial positions and their working paths of the buried plugs.

Path I			Path II		
	History	rev.		History	rev.
a	0 → 3	0.375			
b	0 → 4	0.5	b′	2 → 6	0.5
c	0 → 5	0.625	c′	2 → 7	0.625
d	0 → 6	0.75	d′	2 → 8	0.75
e	0 → 7	0.875	e′	2 → 8+1	0.875
f	0 → 8	1.0	f′	2 → 8+2	1.0
g	0 → 8+1	1.125	g′	2 → 8+3	1.125
h	0 → 8+2	1.25	h′	2 → 8+4	1.25
			i′	2 → 8+5	1.375

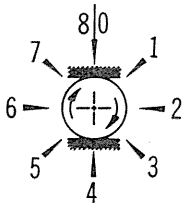

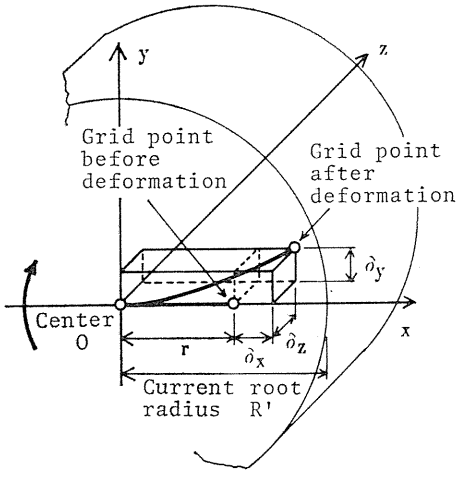

(a) Displacement of a point

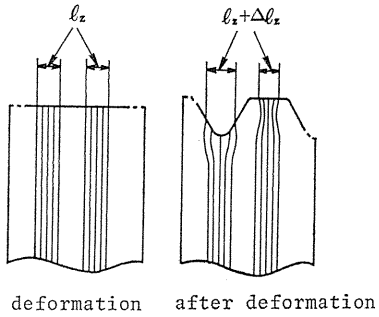

(b) Axial elongation

Fig. 39. Coordinates to represent the movement of a point and the axial strain.

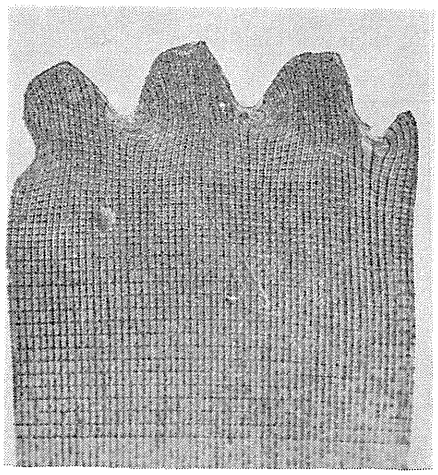

Fig. 40. Example photograph of a deformed grid.

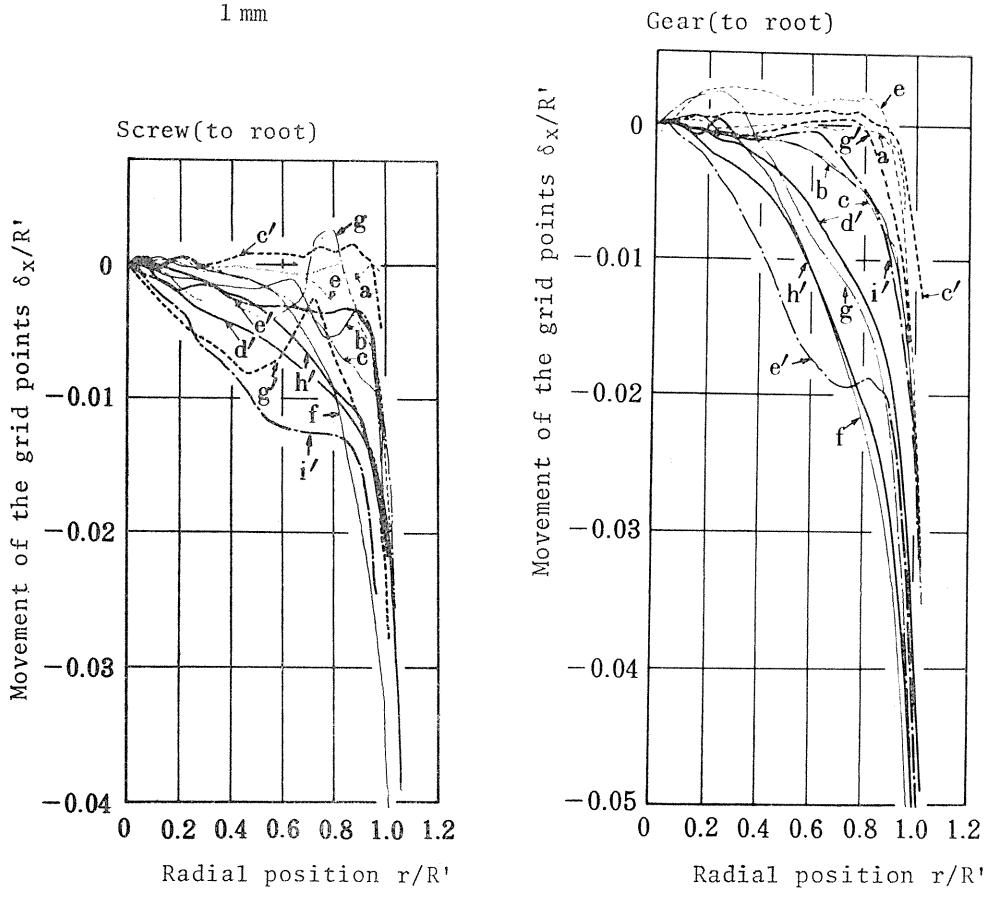

(a) Screw (to root) (b) Gear (to root)

Fig. 41. Movement of the grid point δ_x/R'.

radius (or radius of the root circle) at that stage of rotation and the abscissa means a relative radial position to the same root radii. Notations a to h etc. mean the amount of rotation.

Fig. 42 shows also the deflection of the central grid line in y direction.

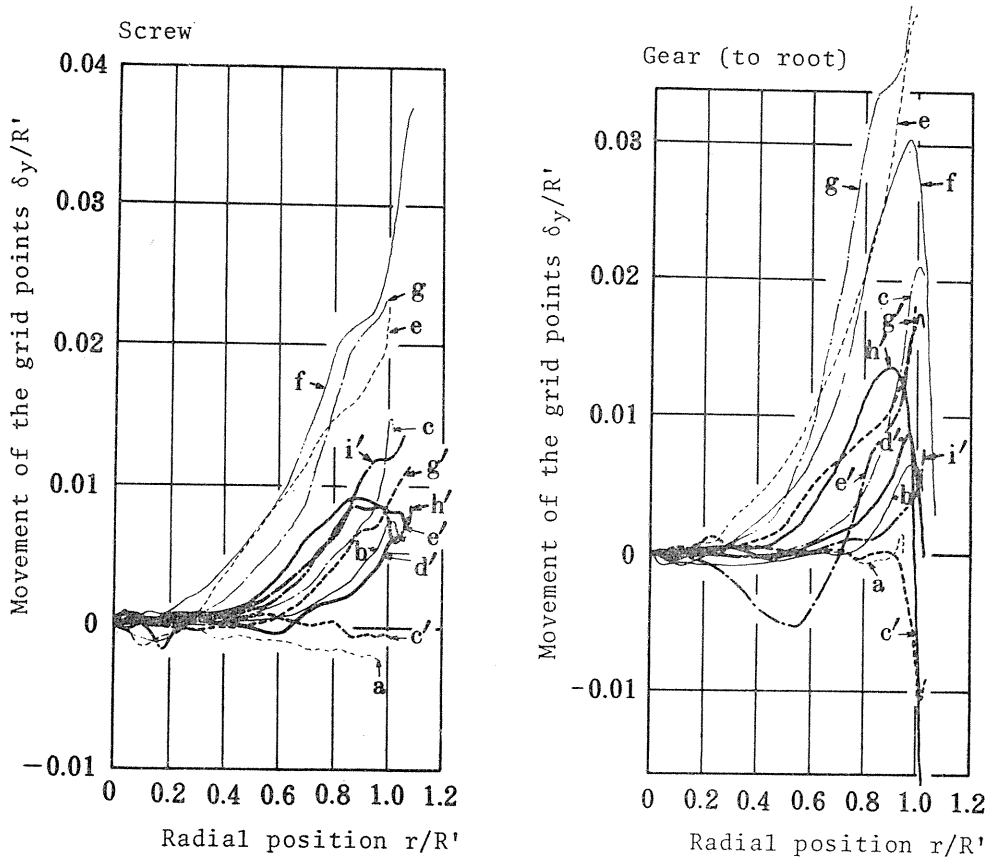

(a) Screw (b) Gear (to root)

Fig. 42. Movement of the grid point δ_y/R'.

Fig. 43 shows the strains at the top and the root of a screw thread and a gear tooth in z direction which are taken from the $\Delta l_z/l_z$'s of meridional grid lines.

As will be seen from these figures, the material suffers vigorous movement when the concerned portion of the specimen passes through the bite portion 0 or 4 (in the path Ⅰ, a to c, in the path Ⅱ, c' to e'). However, the circumstance is fairly the same in the free rotation zone i. e. in the path Ⅰ, c to e, or in the path Ⅱ, e' to g'.

From these observations it will follow that:

(1) The deformation prevails in the specimen on the whole making no exceptions of the central core. It should be noted that in studying the phenomena one

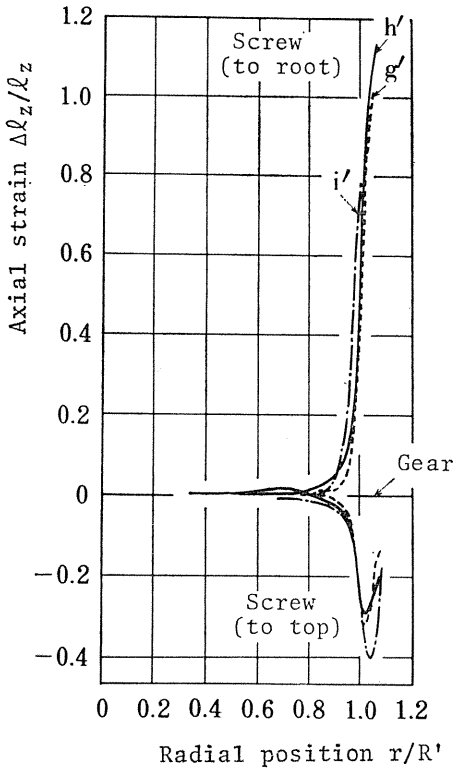

Fig. 43. Axial strain $\Delta l_z/l_z$.

cannot neglect this central core deformation.

(2) Even at a constant final penetration of the dies, material follows different deformation paths according to the initial position occupied when the first bite starts, resulting in a particular ultimate position of material.

(3) Judging from Figs. 41 and 43 distribution trends in δ_x and $\Delta l_z/l_z$ exhibit considerable changes around $r/R'=0.9$ so that in the region of $r/R'<0.9$ the material undergoes a distortion as a whole and in that of $r/R'>0.9$ the material suffers a severe local deformation, thus forming the characteristic feature.

(4) There exist no axial movements of material in the core of the specimen.

From all the above, it appears that a penetration which is imposed by rolling dies cannot be completely utilized for piling up of the feature but a part of it must be consumed for distorting the central core. Consequently, it becomes desirable to know what part of a penetration could be consumed for this central distortion.

5. 5. Compatibility of the feature-formation component and the core-distortion component in a penetration per bite

So far, it has been supposed that a penetration imposed by the dies on the blank cylinder might consist of a core-distortion component and a feature-formation component. In order to discriminate these components in a penetration, attention was paid to the displacement of the radial grid line, in particular to two points on it. They are the surface point and the point at 0.9R′. So, radial movements of

these points appearing in Fig. 41 were taken. They were denoted by δ_x(surface) and $\delta_x(r=0.9R')$ and plotted in the order of paths shown in Table 3. Results are summarized in Fig. 44 and 45. Black circles correspond to the ones representing

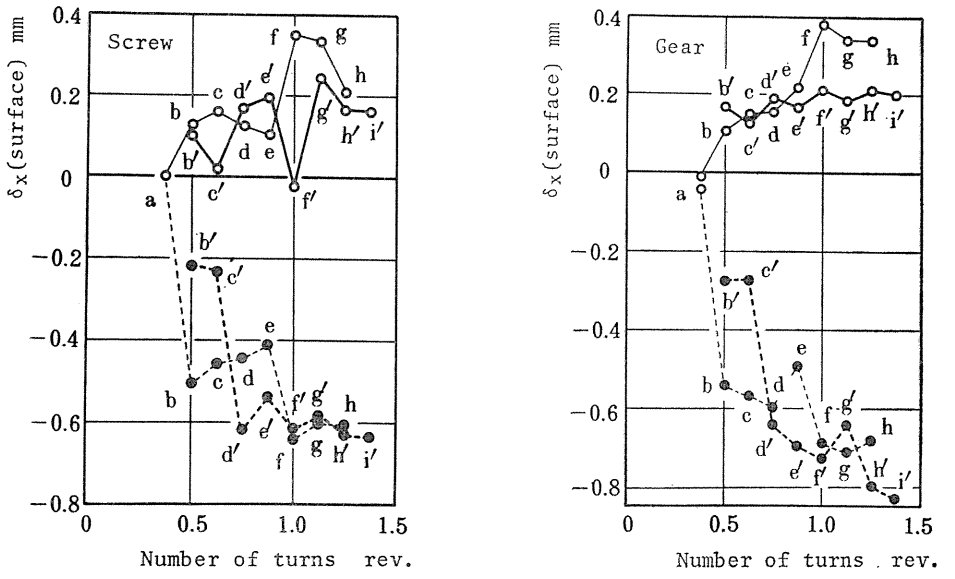

(a) Screw (b) Gear

Fig. 44. Movement of the grid point δ_x(surface).

the root portion of the profile feature and white ones to the tip portion. Thus an ordinate difference in white and black circles means height of the formed profiles. One can realize by these figures how the material behaves with a period of 0.5 revolutions.

Now, referring to the simplified penetration model shown in Fig. 46 any material point on the surface must suffer successive penetrations $(\Delta\delta_x)_t$ at every 0.5 turns. With this penetration per bite the point at 0.9R′ must move an amount of $(\Delta\delta_x)_d$ which would be regarded as the movement consumed by the core distortion. So the difference $(\Delta\delta_x)_t-(\Delta\delta_x)_d$ may be regarded as a penetration component utilized to form the profile features. This penetration component will be referred to as the feature-formation component of penetration and denoted by $(\Delta\delta_x)_p$.

If we consider the path II of a screw, it will be noticed that c' of 0.625 rev. and d' of 0.75 rev., for example, represent the situations of the point before and just after the second bite. So, we can find the penetration per bite in this period to be $(\Delta\delta_x)_t=0.385$mm by reading the ordinate difference between c' and d' of the

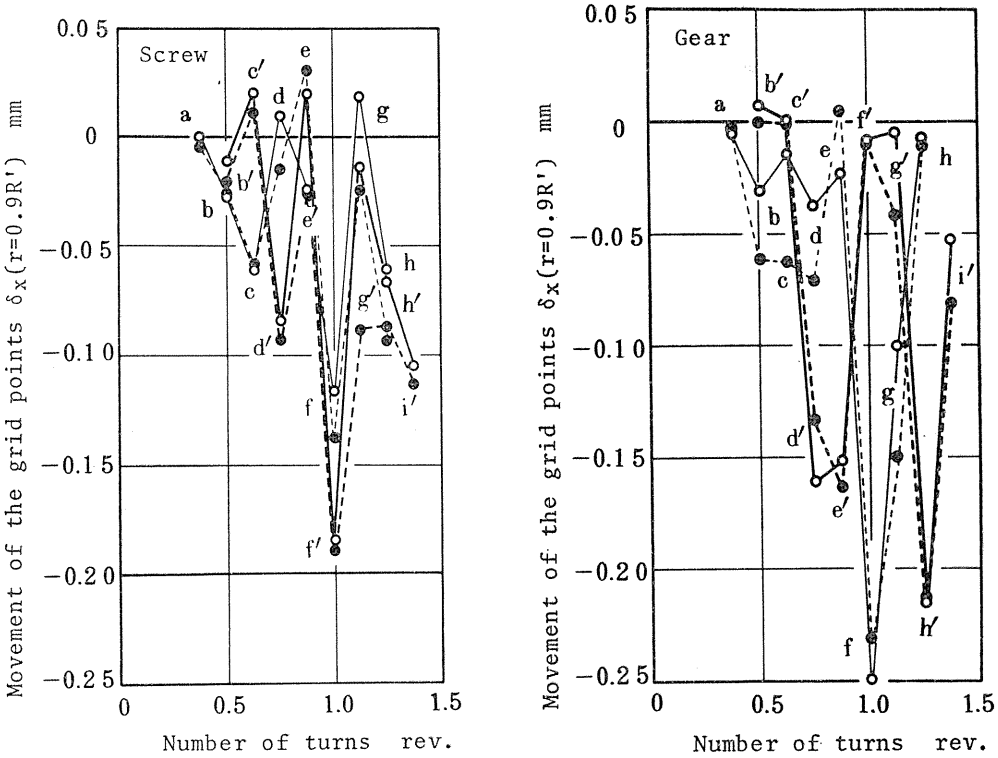

(a) Screw (b) Gear

Fig. 45. Movement of the grid point $\delta_x(r=0.9R')$.
[Marks in the figures: the same as in Fig. 44]

black circles in Fig. 44(a). On the other hand, that of the black or white circles in Fig. 45 should be the core-distortion component in this period, i. e. $(\Delta\delta_x)_d = 0.105$ mm. Consequently, we can obtain the feature-formation component $(\Delta\delta_x)_p$ in this period as follows. $(\Delta\delta_x)_p = (\Delta\delta_x)_t - (\Delta\delta_x)_d = 0.385 - 0.105 = 0.280$ mm. Applying similar considerations to the period of *a* to *b*, *e* to *f*, etc., both components of penetration of the screw in the process can be given in Fig. 47. Supposing that an observer stands on the spatial point 0 or 4 and observes how the balance of $(\Delta\delta_x)_p$ and $(\Delta\delta_x)_d$ fluctuates as the material points are successively passing through this biting portion, he can find that the plots of $(\Delta\delta_x)_p$ and $(\Delta\delta_x)_d$ against the number of turns become the ones as given in Fig. 47. In this figure, particularly, $\sum(\Delta\delta_x)_p$ is also plotted by adding up the penetrations per bite of every 0.5 revolutions. Applying these values of $\sum(\Delta\delta_x)_p$ instead of $\sum(\Delta\delta_x)_t$ to the process models proposed in Chapter 4, we can estimate the feature-forming-ratio ϕ as indicated with

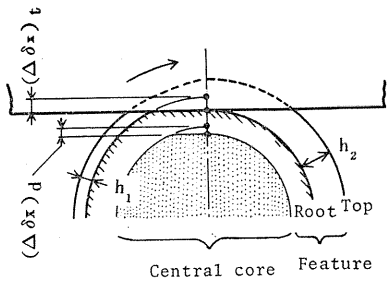

$(\Delta\delta x)_p = (\Delta\delta x)_t - (\Delta\delta x)_d$, $\Delta h = h_2 - h_1$

Fig. 46. Simplified penetration model.

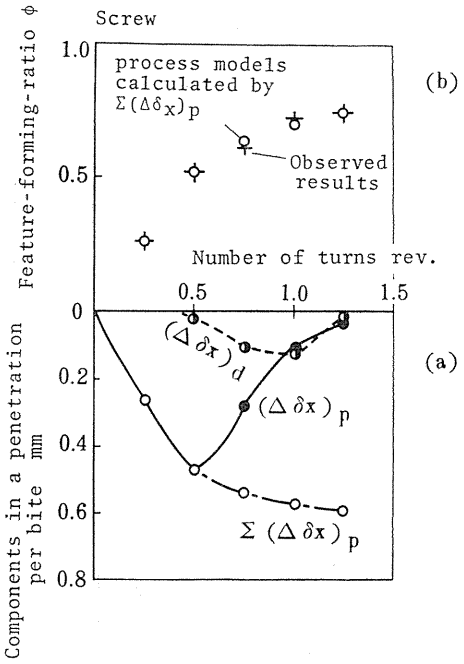

Fig. 47. Components in a penetration per bite and feature-forming ratio (screw).

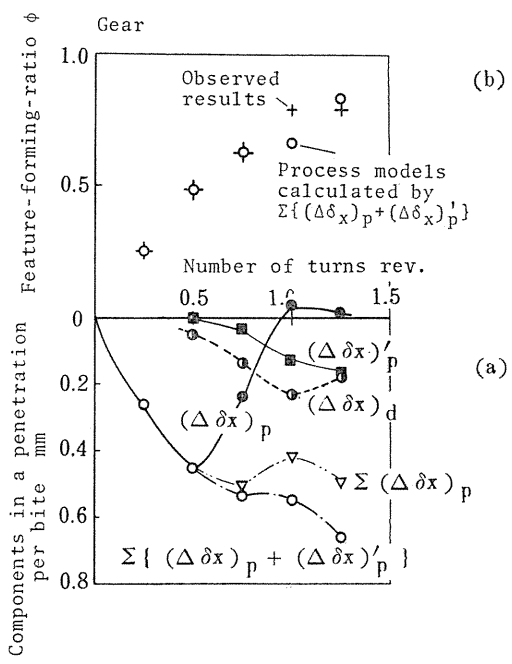

Fig. 48. Components in a penetration per bite and feature-forming ratio (gear).

the small circles in (b) of the same figure, which shows good agreement with the observed results of + mark. The value of ϕ is given by $\phi=h/h_f$, where h is the current height of a thread and h_f the final must-height.

Fig. 48 shows a similar diagram for the gear. But, in this case, since the forming action is still effective in the receding side, $\sum\{(\Delta\delta_x)_p+(\Delta\delta_x)_{p'}\}$ can well be utilized to predict the feature-forming-ratio, where $(\Delta\delta_x)_{p'}$ is the feature-formation component corresponding to the receding side.

Now, let us consider the cross-sectional profile of the components. Combining the core-distortion component of $(\Delta\delta_x)_d$ with the result obtained by the plastic kneading of plain cylinders (Chapter 3), one can predict the contact width in cross section as follows. Assuming that the central core of the component does not deform at all, nominal value of contact width of w' between tools and material can be estimated by a simple geometry shown in Fig. 49 (a) which has no contact region in the receding side. Nominal contact widths of the screw are also calculated by taking measured value of $(\Delta\delta_x)_t$ as $(D_0-D_{min})/2$ in Fig. 49 (a). The result is represented in Fig. 50 by small white circles. As referred to in Chapter 3, in the case of the plastic kneading, contact widths of w can be plotted as a full line in Fig. 49(b). The nominal value of w' above estimated becomes smaller than this w as shown in the same figure. The values of $(w-w')$ should be thought as a modification introduced by the plastic deformation of the central core. Considering that the reduction in Fig. 49(b) corresponds to $(\Delta\delta_x)_d/R'$ in this case, we are able to have plots of the modification value of the screw as small black circles in Fig.

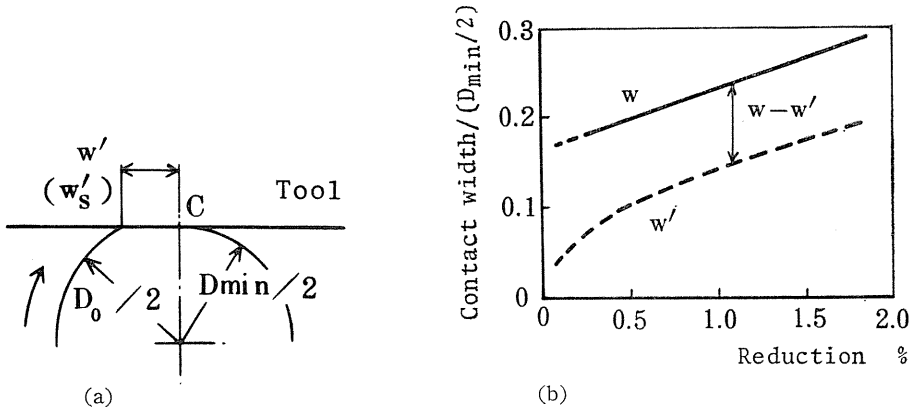

Fig. 49. Nominal contact width and its modification.

50. Full line in Fig. 50 represents the estimated values of the contact widths thus obtained. They agree with the observed values[17] marked △.

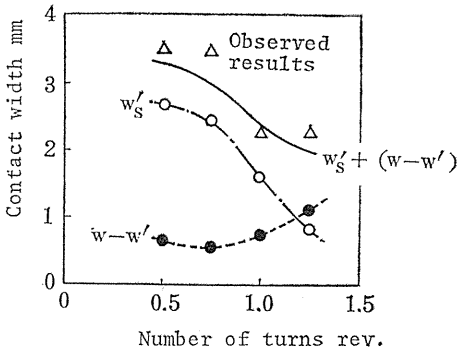

Fig. 50. Contact width of the screw.

After all, the determinant factor which really concerns the piling up of the profile feature is not the whole penetration per bite of $(\Delta\delta_x)_t$ but $(\Delta\delta_x)_p$ of the feature-formation component. So the difference, $(\Delta\delta_x)_t-(\Delta\delta_x)_p=(\Delta\delta_x)_d$, is consumed for the core distortion. The balance and magnitude of the feature-formation component and the core-distortion component vary with the rolling conditions and the rolling stages, and the compatibility of both components determines the formation rate of the feature, distortion of the core and the contact region between the tools and material. Though the technique to resolve the die penetration into two components is an expedient, it is useful to analyze the deformation and predict the form of the products. Next we will consider the mechanics which determine the compatibility of these components

5. 6. Rolling forces

The normal reaction and tangential driving force observable in the rolling of a screw and a gear, are exemplified in Fig. 51 (a) and (b). The force diagram of the gear shows a similar tendency to the screw, except that the gear has some pulsation in its force curves corresponding to the tooth to tooth interval. The maximum value of the tangential force, which is seen after initial revolutions of 0.8~0.9, is avout 20% of that of the normal one. It should be noted that the F/W values in these cases are far larger than in the rolling of plain cylinder between flat dies.

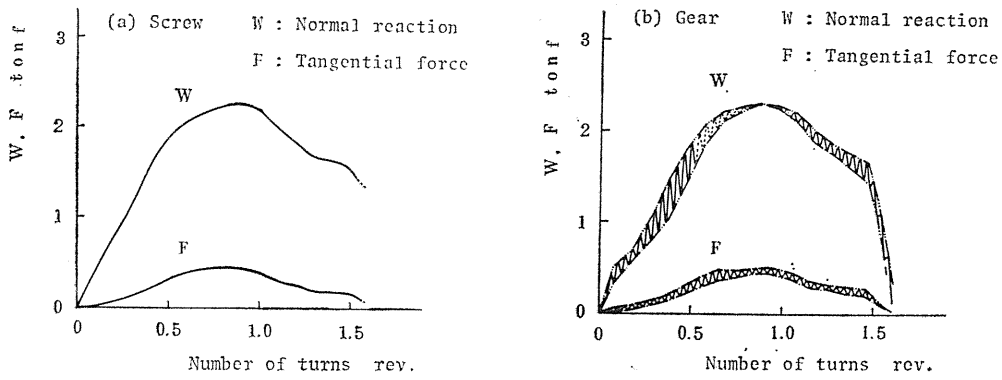

(a) Screw (b) Gear

Fig. 51. Normal reaction and tangential driving force.

5. 7. *Consideration of the relationship between the normal reaction and the penetration components*

At a stage of rolling, if the material is imposed by a certain amount of die penetration, the normal reaction per unit length would be, for example, raised to a level of S–T line in Fig. 52. In this case, suppose the central core of a specimen defies the plastic deformation, then the die penetration upon the surface should be wholly utilized for piling up of the feature, and a load-die penetration curve would be represented qualitatively by a two-dot chain line OP which is referred to as the "feature-formation curve". On the other hand, if all the die penetration were absorbed in distorting the central core without any additive forming of the feature at all, then a load curve would be represented by a broken line OD which will be referred to as the "core-distortion curve". In the actual rolling, both the feature and the core deformation must coexist so that two components caused by a penetration of $(\Delta\delta_x)_t$ are SP for $(\Delta\delta_x)_p$ and SD for $(\Delta\delta_x)_d$. And $(\Delta\delta_x)_t$ is equal to ST, i. e. SP+SD. In this representation we find ourselves in a situation of having sufficient data for plotting D's and P's drawn from results of experiment at various rolling stages. Fig. 53 shows the plots of D's which seem to agree with the result of rolling plain cylinders between flat dies (solid line). In the next graphical step

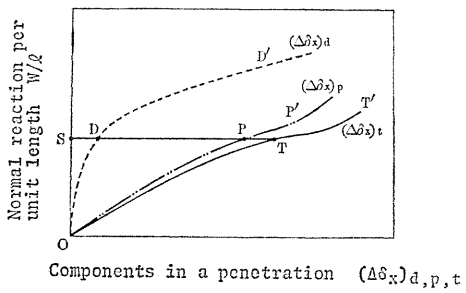

Fig. 52. W/l-$(\Delta\delta_x)_{d,p,t}$ curve (qualitative diagram).

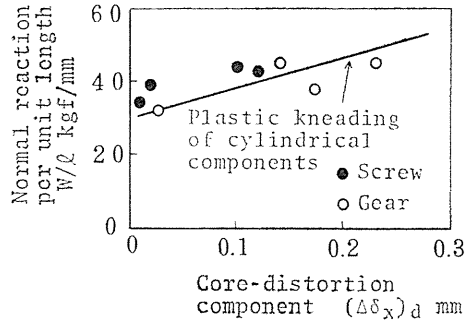

Fig. 53. W/l-$(\Delta\delta_x)_d$ curve.

to determine P's, it is convenient to superpose P on D as a point by changing the abscissa of $(\Delta\delta_x)_p$, right to left. In this way, Fig. 54 and Fig. 55 represent such constitution diagrams which visualize the mechanics inherent in the components-rolling. In these figures, the origin of a core-distortion curve is denoted by a

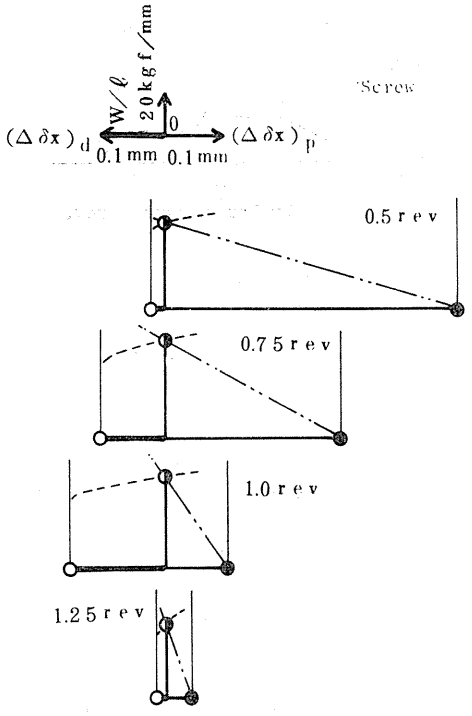

Fig. 54. Compatible point of the normal reactions for two components in a penetration (screw).

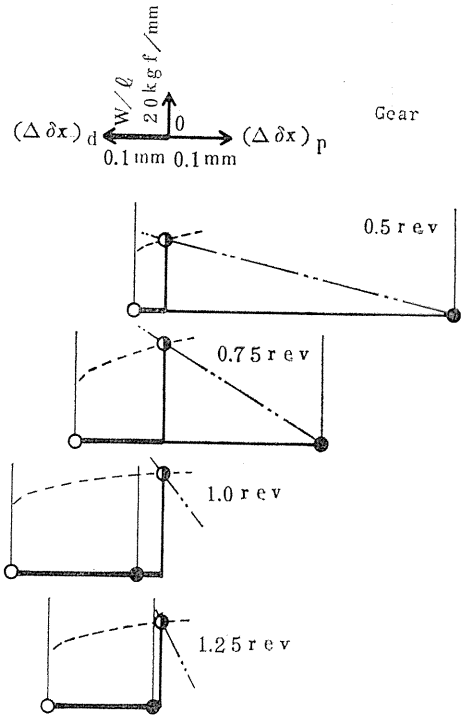

Fig. 55. Compatible point of the normal reactions for two components in a penetration (gear).

○ Origin of the core-distortion curve

● Origin of the feature-formation curve

◑ Compatible point

small white circle, and that of a feature-formation curve by a small black one, and a consistent load value common to both curves is shown by a half black circle. Though the details of the feature-formation curves are not shown here, we can see the deformation characteristics in the rolling process through the load required, which are affected not only by the aimed feature but also by the stage of rolling. It is observed that $(\Delta\delta_x)_p$ takes negative values in some gears when the tooth profile formed by the preceding bite needs a larger modification.

5. 8. Core-distortion curves and feature-formation curves[18]

As described above, the constitution diagram of a core-distortion curve and a feature-formation curve, which is a powerful technique for solving complex plastic

flow problems of the components-rolling, is introduced. It is important, therefore, to examine all details of these curves. Consequently, the current section is devoted to the determination of core-distortion curves and feature-formation curves.

In this case, thread rolling machine with two cylindrical dies was utilized and some sophisticated procedure was taken to draw out these curves. In experiment, an aluminium specimen was pre-rolled to some stage of the process under the condition which minimized the deformation of core. The pre-formed specimen was rolled again to suffer an additional penetration of dies. Before and after an additional penetration the profile of the specimen was measured by a toolmakers' microscope with a precision angular dividing attachment and a tracer-type form tester, while the normal component of the rolling force acting on the die face was caught throughout a process by a tie-rod which connects opposed die-heads. The feature-formation component $(\Delta\delta_x)_p$ of an additional penetration of dies can be estimated by the piled-up height of a feature based on the assumptions of

Table 4. Experimental conditions (thread rolling machine)

thread rolling machine	maximum rolling force : 20 tonf revolving speed of dies : 0.85 rpm
tools (dies)	diameter : 180 mm pitch : 2 mm lead angle : 0°
blank	material : aluminium A1050F diameter : 16.52 mm length : 50 mm
product	screw-like component
lubricant	not used

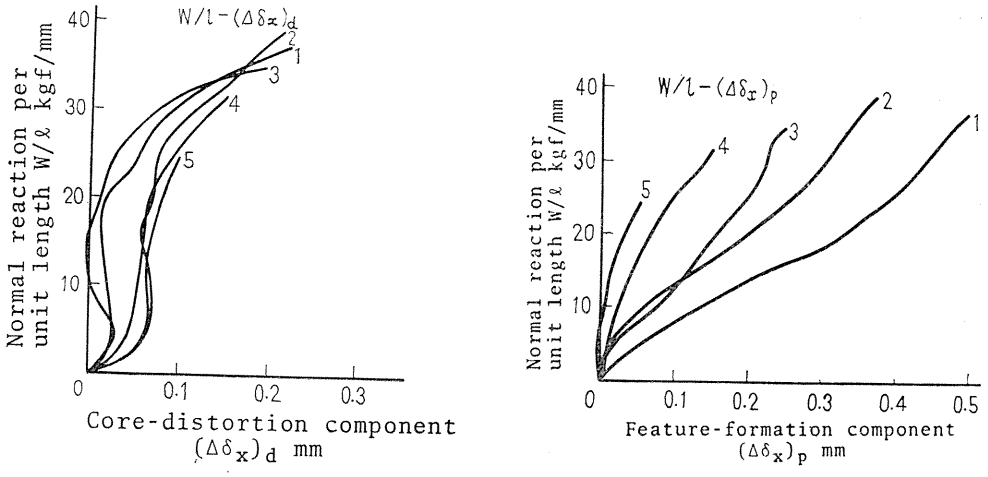

(a) Core-distortion curves (b) Feature-formation curves.

Fig. 56. All details of the characteristic curves.

process models in Chapter 4. Consequently, we can also find the core-distortion component $(\Delta\Delta_x)_d$ in this period as $(\Delta\delta_x)_d = (\Delta\delta_x)_t - (\Delta\delta_x)_p$. The specifications of the thread rolling machine, tools, material used, and other experimental conditions are tabulated in Table 4, and results obtained are summarized in Fig. 56. The numbers of curves in Fig. 56 correspond to those in Fig. 57 which shows the pre-forming stages and the additional penetrations taken in this experimental rolling.

As will be seen in Fig. 56, the core-distortion curves follow the same path at any stage of rolling, whereas the slope of a feature-formation curve becomes steeper as the rolling process goes on.

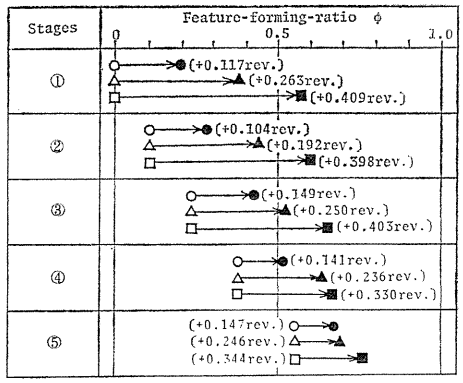

Fig. 57. Pre-forming stages and additional penetrations.

5. 9. Summary

By means of applying the split plug to an analysis of a three dimensional flow taking place in the material, it becomes possible to attain a consistent understanding of the phenomena encountered in the process of components-rolling.

The results obtained are summarized as follows:

(1) The split plug method employed in the experiments is useful for detecting a three dimentional pattern of the material flow throughout the workpiece.

(2) The deformation prevails in the specimen on the whole making no exceptions of the central core. Even in a constant final penetration of the dies, the material follows different deformation paths according to the initial position occupied when the first bite starts.

(3) In the region of $r/R' < 0.9$ of radial position the material undergoes a distortion as a whole and in that of $r/R' > 0.9$ the material suffers a severe local deformation, thus forming the characteristic feature.

(4) A penetration $(\Delta\delta_x)_t$ imposed by the dies on the blank cylinder is found to consist of two components, a core-distortion component $(\Delta\delta_x)_d$ and a feature-formation component $(\Delta\delta_x)_p$. The balance and magnitude of $(\Delta\delta_x)_d$ and $(\Delta\delta_x)_p$ vary with the rolling conditions and the rolling stages.

(5) A current height of the feature can be estimated by the calculation of the process models adopting the feature-formation component in a penetration for the nominal penetration.

(6) Combining the core-distortion component with the result of Chapter 3, plastic kneading of the cylindrical components, contact width between the dies and the screw can be estimated.

(7) Since the balance of the core-distortion component and the feature-formation component should be self-determined through the load required, the mechanics inherent in the components-rolling is constructed and visualized from the experimental results.

(8) All details of the core-distortion curves and feature-formation curves were exemplified in the case of thread rolling. While the core-distortion curve follows the same path at any stage of rolling, the slope of a feature-formation

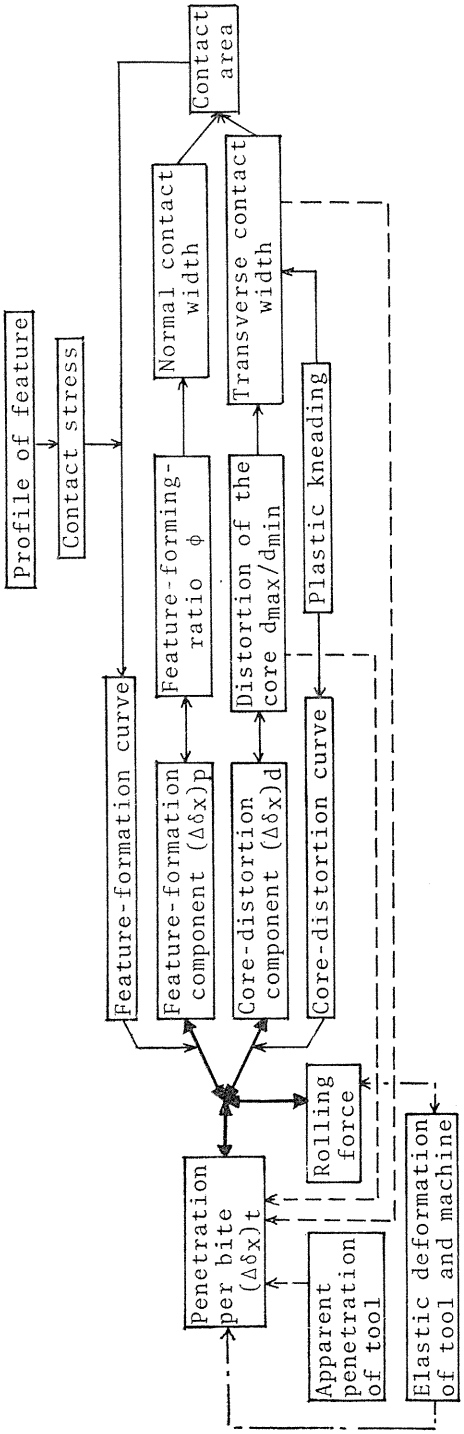

Fig. 58. Interrelation diagram.

curve becomes steeper as the rolling process goes on.

6. Conclusions

The investigation reveals a detailed mechanism of deformation in the components-rolling. The factors referred to in this paper are related to each other through the diagram shown in Fig. 58[19]. In this diagram four thick lines show a compatible condition which is settled down in accordance with the mechanics inherent in the components-rolling. Attention should be paid to the loops of thin lines and, among others, to the core-distortion component $(\Delta\delta_x)_d$. There are also complicated circumstances behind the penetration per bite $(\Delta\delta_x)_t$ as will be seen from broken lines. On the basis of this diagram, the consistent picture of a rolling process will be visualized.

Acknowledgement

The author would like to thank Emeritus Professor Y. Kasuga for his useful suggestions and discussions. The author also wishes to thank Professor S. Kato and Professor N. Kawai for their helpful advices.

Appendix

The estimation for the distribution of the normal components of stress can be done by the following technique if the process is in a steady state. As in Fig. 59, the sensitive plane of the pressure pin is supposed to be divided into n elements which have an equi-width dw, and the area dA_i (i=1, 2, 3, ... n). The working area of the normal component of stress can be also divided into the same width dw with corresponding pressure p_j (j=1, 2, 3, ... m). The load carried by the pressure pin at various stages of the process, W_{pk} (k=1, 2, 3, ... m+n−1), will be represented by the equations in Fig. 59. In these equations, W_{pk} can be obtained by the records and dA_i can be given by geometrical calculation. Thus, we can estimate p_j's uniquely. For the case of Fig. 16, dw=0.1 mm was taken.

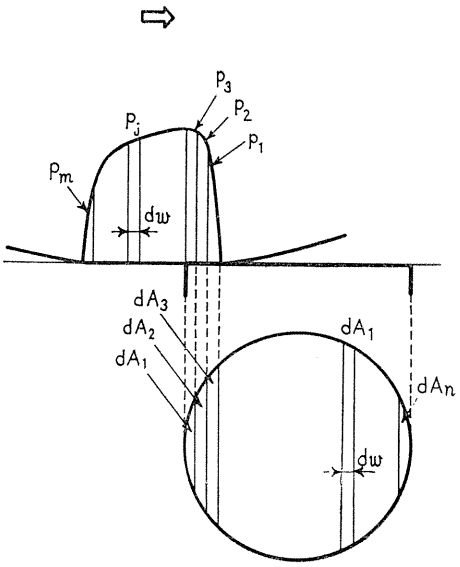

$$W_{p_1}=dA_1\times p_1 \quad \cdots\cdots(1)$$
$$W_{p_2}=dA_1\times p_2+dA_2\times p_1 \quad \cdots\cdots(2)$$
$$W_{p_i}=\sum_{j=1}^{j} dA_j\times p_{i-j+1} \quad \cdots\cdots(i)$$
$$W_{p_{m+n-1}}=dA_n\times p_m \cdots\cdots(m+n-1)$$

Fig. 59. Method of estimation of the pressure distribution.

References

1) For example:
Yamamoto, A., Jour. Japan Soc. Mech. Engrs., Vol. 51, No. 305 (1948-8, 9), p. 335; Masuda, M., Jour. Japan Soc. Precision Engng., Vol. 19, No. 4 (1953-4), p. 143; Drăghich, G., et al., Werkstatt u. Betr., 104 Jg. Heft 10 (1971-10), S. 755.
2) For example:
Hayama, M., Jour. Japan Soc. Technol. of Plasticity, Vol. 9, No. 86 (1968-3), p. 190; Yamamoto, A. and Kasai, S., Trans. Japan Soc. Mech. Engrs., Vol. 37, No. 296 (1971-4), p. 834.
3) Masuda, M., Jour. Japan Soc. Technol. of Plasticity, Vol. 14, No. 145 (1973-2), p. 116.
4) For example:
Tsuchikawa, T., Trans. Japan Mech. Engrs., Vol. 27, No. 175 (1961-3), p. 329; Inoue, K., et al., Jour. Japan Soc. Precision Engng., Vol. 41, No. 9 (1975-9), p. 866.
5) For example:
Awano, T. and Danno, A., Jour. Japan Soc. Technol. of Plasticity, Vol. 9, No. 88 (1968-5), p. 296.
6) Sugiyama, H., Annals of the CIRP, Vol. 22, No. 1 (1973-8), p. 93.
7) Yokoyama, K. and Yamamoto, A., Sci. of Machine, Vol. 10, No. 9 (1958-9), p. 1093; Naruse, M., Deformation processings of Gears, (1963), Yokendo; Awano, T. and Danno, A., Jour. Japan Soc. Technol. of Plasticity, Vol. 9, No. 88 (1968-5), p. 285; Maekawa, Y., Preprint of 1975's Japanese Spring Conf. for Deformation Processings, (1975-5), p. 157.
8) Tsutsumi, S. et al., Bull. JSME, Vol. 20, No. 150 (1977-12), p. 1640.
9) For example:
Агамирзян, Л. С. и Ломсадзе, Дж. М., Известия высших учебных заведений черная металлургия, No. 11 (1969), с. 114.
10) Kasuga, Y., et al., Preprint of Japan Soc. Mech. Engrs., No. 713-6 (1971-11), p. 73.
11) Kato, K., et al., Preprint of 1975's Japanese Spring Conf. for Deformation Processings, (1975-5), p. 153.
12) Hayama, M., Jour. Japan Soc. Technol. of Plasticity, Vol. 15, No. 157 (1974-2), p. 141.
13) For example:
Merwin, J. and Johnson, K. L., Proc. Inst. Mech. Engrs., Vol. 177, No. 25 (1963), p. 676; Hamilton, G. M., Proc. Inst. Mech. Engrs., Vol. 177, No. 25 (1963), p. 667.
14) Kudo, H. and Nagahama, T., Jour, Japan Soc. Technol. of Plasticity, Vol. 10, No. 106 (1969-11), p. 837.
15) Tsutsumi, S. et al., Bull. JSME, Vol. 23, No. 175 (1980-1), p. 110.
16) Tsutsumi, S. et al., Bull. JSME, Vol. 23, No. 175 (1980-1), p.118.
17) Kasuga, Y. et al., Preprint of 27th Conf. for Deformation Processings, (1976-11), p. 148.
18) Tsutsumi, S. and Goto, K., Preprint of 1979's Japanese Spring Conf. for Deformation Processings, (1979-5), p. 135.
19) Tsutsumi, S., Jour. Japan Soc. Mech. Engrs., Vol. 84, No. 748 (1981-3), p. 250.